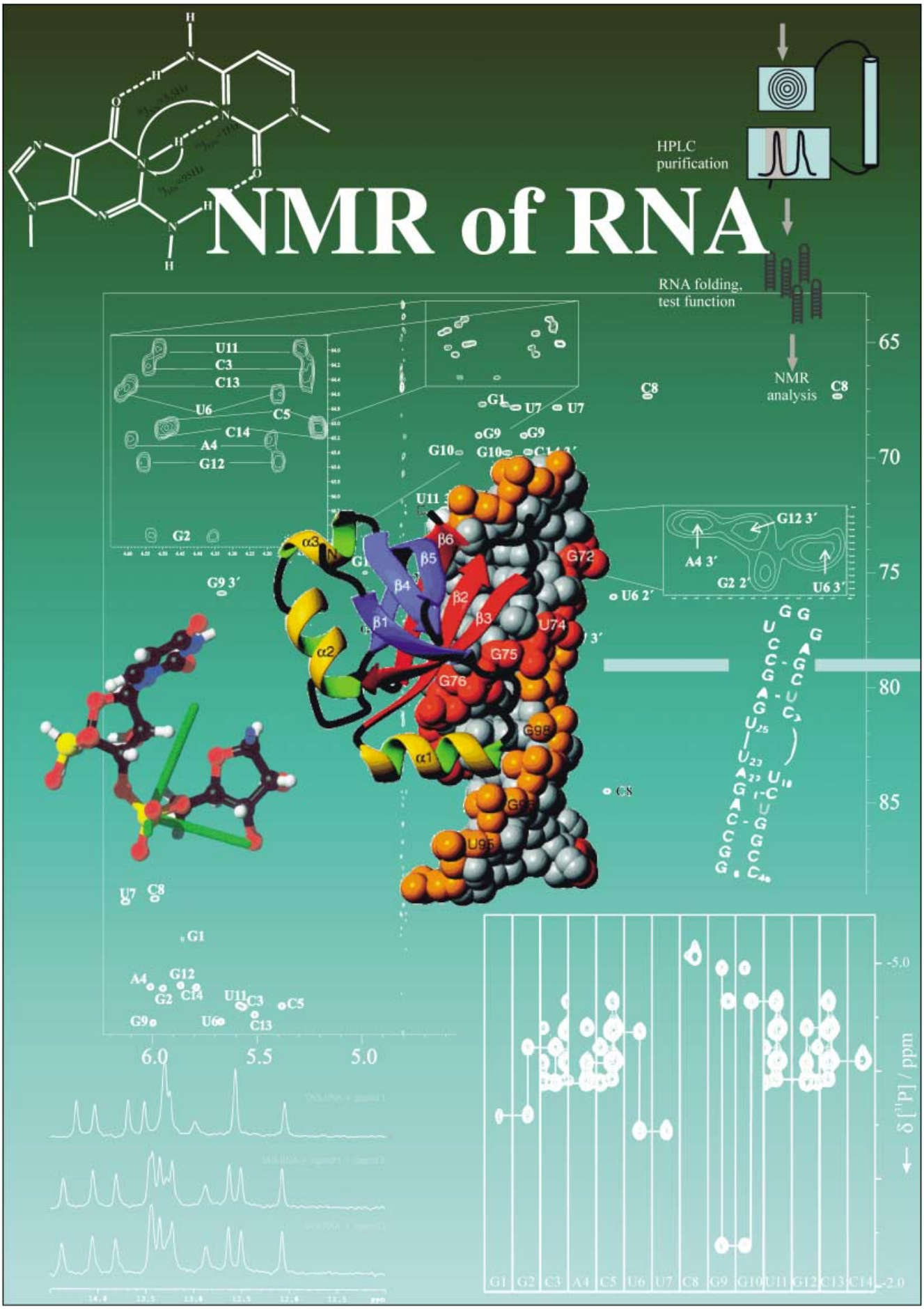

 © 2003 Wiley-VCH Verlag GmbH & Co. KGaA, Weinheim DOI: 10.1002/cbic.200300700

NMR Spectroscopy of RNA

Boris Fürtig, Christian Richter, Jens Wöhnert, and Harald Schwalbe*[a]

NMR spectroscopy is a powerful tool for studying proteins and nucleic acids in solution. This is illustrated by the fact that nearly half of all current RNA structures were determined by using NMR techniques. Information about the structure, dynamics, and interactions with other RNA molecules, proteins, ions, and small ligands can be obtained for RNA molecules up to 100 nucleotides. This review provides insight into the resonance assignment methods that are the first and crucial step of all NMR studies, into the determination of base-pair geometry, into the examination of local and global RNA conformation, and into the detection of interaction sites of RNA. Examples of NMR investigations of RNA are given by using several different RNA molecules to illustrate the information content obtainable by NMR spectroscopy and the applicability of NMR techniques to a wide range of biologically interesting RNA molecules.

1. Introduction

NMR spectroscopy is a powerful tool for studying the structure and dynamics of RNA molecules in solution and their interactions with ligands such as proteins, other nucleic acids, molecules of low molecular weight, ions, and solvent molecules. Up to now, nearly half of all three-dimensional structures of nucleic acids have been solved by NMR spectroscopy.

Within the current size limits of NMR measurements on RNA (about 100 nucleotides for information with intermediate resolution and 50 nucleotides for high-resolution structure characterization), there is a plethora of information that can be derived from NMR spectroscopic studies:

- The base-pairing pattern. This includes standard and non-standard Watson–Crick-type base pairs and allows verification and prediction of the secondary structure elements of RNA (discussed in Section 3) and determination of the base-pair dynamics.
- Information about conformational equilibria, such as those between hairpin and duplex structures (Section 4).
- Site-specific information about ion binding to RNA (Section 5).
- NMR spectroscopy resonance assignment of RNA (Section 6) and analysis of chemical shifts (Section 7).
- Delineation of secondary structure motifs, such as hairpins and bulges (Section 8).
- The local structure and dynamics (Section 9) and global structure of RNA derived from residual dipolar couplings (Section 10).
- Mapping of the interaction surfaces of RNA with small ligands, other RNA molecules, or proteins (Section 11).

The introduction of methods for the preparation of milligram quantities of RNA in an isotope-labeled (^{13}C,^{15}N) form has been a prerequisite for all of these NMR studies and biochemical methods. The preparation of milligram quantities of RNA is discussed in Section 2.

With isotope-labeled RNA at hand, the first step is to assign every NMR-active atom (^{1}H, ^{13}C, ^{15}N, ^{31}P) in the molecule to its respective resonance in the NMR spectra; this is followed by interpretation of NMR parameters such as NOE contacts, *J* couplings, residual dipolar couplings, and cross-correlated relaxation rates for the determination of a three-dimensional structure. Resonance assignment in NMR spectroscopy is more difficult for RNA than for proteins. In comparison to proteins, the chemical-shift dispersion in the spectra of RNA, a biopolymer made out of only four different nucleotides, is significantly reduced. In addition, the A-form helix is the sole dominating secondary structure element found in RNA. Therefore, many nucleotides experience a similar chemical environment in helical secondary structures which, as a consequence, causes similar chemical shifts. Chemical-shift dispersion is often only observed in noncanonical structural elements such as hairpins, bulges, or internal loops.

The limited chemical-shift dispersion can be overcome by the examination of appropriately sized modular secondary structure elements (see Section 8) that are often involved in molecular recognition, whereas the canonical A-form helical elements frequently serve as a scaffold. In addition, the application of multidimensional heteronuclear NMR experiments (for example, as reviewed by Varani et al.[1] and by Wijmenga and van Buuren[2]) to completely or selectively isotope-labeled RNA molecules[3–5] increases the resolution observed in NMR experiments by the combination of a proton chemical-shift dimension with one or two heteronuclear chemical-shift dimensions.

In this review, we introduce NMR experiments that use a 14-mer RNA cUUCGg tetraloop as a model system with high spectral resolution (Figure 1).[6] The cUUCGg tetraloop is well character-

[a] *H. Schwalbe, B. Fürtig, C. Richter, J. Wöhnert*
Institute for Organic Chemistry and Chemical Biology
Center for Biomolecular Magnetic Resonance
Johann Wolfgang Goethe University
Marie-Curie-Strasse 11, 60439 Frankfurt am Main (Germany)
Fax: (+49) 69-798-29515
E-mail: schwalbe@nmr.uni-frankfurt.de

 DOI: 10.1002/cbic.200300700 © 2003 Wiley-VCH Verlag GmbH & Co. KGaA, Weinheim

Left to right: B. Fürtig, H. Schwalbe, J. Wöhnert, C. Richter.

Harald Schwalbe, born in 1966, studied chemistry in Frankfurt at the Johann Wolfgang Goethe University and received his diploma and PhD thesis in the group of Prof. Griesinger. He was a postdoctoral fellow in the group of Prof. Dobson at the University of Oxford, UK, and then worked at the University of Frankfurt as a Habilitand from 1996 – 1999. In 1999, he moved to the Massachusetts Institute of Technology (MIT), Cambridge, USA, where he was first Assistant Professor and then Associate Professor in the Department of Chemistry. In 2001, he became a full professor for organic chemistry in Frankfurt. His research interests focus on the determination of structure, dynamics, and functions of proteins and RNA by using high-resolution NMR spectroscopy.

Jens Wöhnert, born in 1970, studied biochemistry at the Martin Luther University, Halle/Saale, and graduated in 1996. He obtained his PhD at the Institute of Molecular Biotechnology, Jena, where he applied NMR spectroscopy to study the structure of RNA and RNA – protein complexes. In 2000, he joined the group of Prof. Schwalbe at the Francis Bitter Magnet Laboratory at MIT. Since 2003, he has been a group leader in the SFB 579 "RNA – Ligand Interactions" at the Johann Wolfgang Goethe University, Frankfurt.

Christian Richter, born in 1970, studied chemistry at the Johann Wolfgang Goethe University, Frankfurt, where he graduated in 1996. He obtained his PhD in Frankfurt in the research group of Prof. Griesinger where he developed new NMR pulse sequences for the structure calculation of RNA. In 1999, he joined the application laboratory at Bruker BioSpin, first in Rheinstetten and then in 2000 at Fällanden, Switzerland. During this time, the main focus of his work was participation in the development of the CryoProbe. Since 2002, he has held a permanent position and is responsible for the NMR spectrometers and the NMR training of the researchers in the group of Prof. Schwalbe at the Johann Wolfgang Goethe University.

Boris Fürtig, born in 1978, studied biochemistry in Frankfurt and received his diploma in the group of Prof. Schwalbe in spring 2003. He is now working towards a PhD in the group of Prof. Schwalbe. His work is focused on the investigation of RNA by NMR spectroscopic methods.

ized both by NMR spectroscopy and by X-ray crystallography.[7, 8] It is extremely stable[9] and frequently found in nature. It can also be considered as a secondary structure building block incorporated into many larger RNA structures (see Section 8). It consists of a five-base-pair A-form helix closed by the four loop nucleotides UUCG (Figure 2). In addition, spectra for a number of different RNA systems, including a 10-mer RNA containing a dynamic cUUUUg tetraloop, a double-stranded 16-mer RNA containing a tandem G:A mismatch, a secondary structure element of the 5S rRNA containing a cUUCGg tetraloop, and a 30-mer RNA derived from the coxsackie virus are also shown for comparison.

2. Preparation of Isotope-Labeled RNA

The restricted resolution of NMR spectra of RNA makes the introduction of stable ^{13}C,^{15}N isotopes an attractive tool for improving the quality of RNA structures determined by NMR spectroscopy. There are currently both biochemical and chemical methods (reviewed by Kojima et al.[10] and by Lagoja and Herdewijn[11]) for the synthesis of isotope-labeled RNA. The main advantages of chemical synthesis and subsequent phosphoramidite chemistry for the synthesis of the oligonucleotides are the selective incorporation of labeled nucleotides at specific positions of interest (see Figure 3 as an example[12]) and the possibility to incorporate nonstandard nucleobases, which are quite often found in RNA.

However, ^{13}C,^{15}N-labeled precursors for the chemical synthesis of completely labeled RNA molecules are expensive and difficult to synthesize. Therefore, enzymatic in vitro transcription with DNA-dependent RNA-polymerases such as T7-, T3-, or SP6-RNA-polymerase[13–17] has become the method of choice in many groups for the synthesis of ^{13}C,^{15}N-labeled RNA molecules. The most widely used polymerase is the T7-RNA-polymerase. Besides nucleotide triphosphates in an appropriately labeled form, the polymerase requires a DNA template. Linearized plasmids, synthetic double-stranded DNA, or single-stranded DNA with a double-stranded promoter region can serve as DNA templates (Figure 4). In general, linearized plasmids or double-stranded DNA appear to be more effective templates. There are certain

 © 2003 Wiley-VCH Verlag GmbH & Co. KGaA, Weinheim

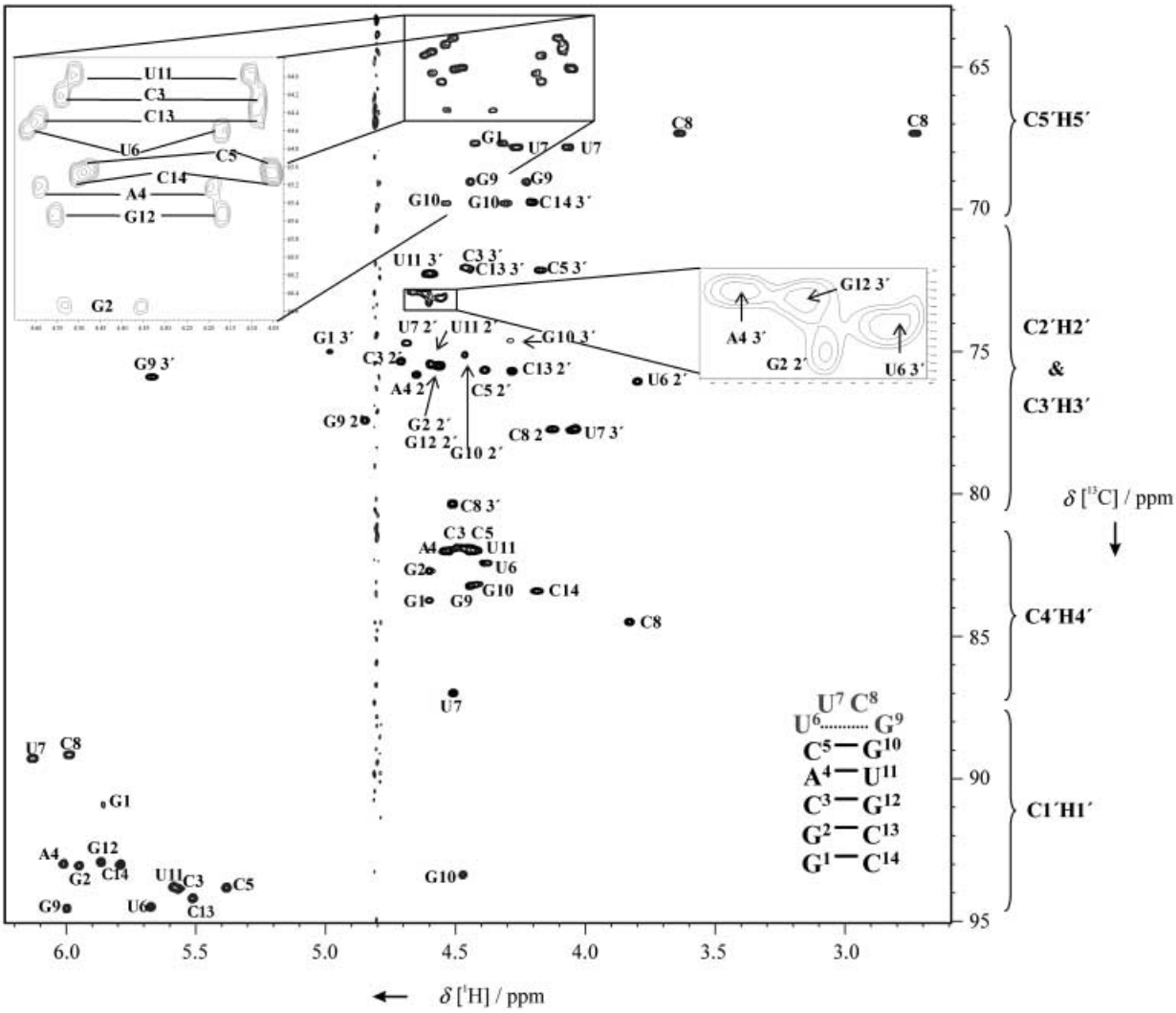

Figure 1. $^{1}H,^{13}C$-CT-HSQC spectrum of the cUUCGg tetraloop at 600 MHz. The assignments of the C1′H1′ – C5′H5′/H5″ atoms of the sugar moiety are indicated.

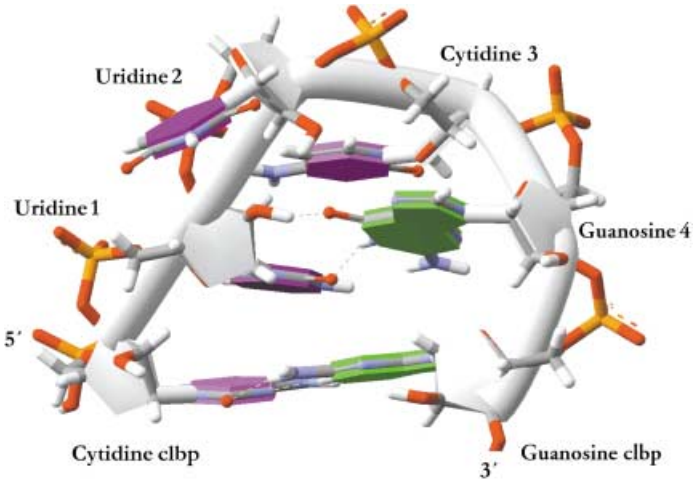

Figure 2. The UUCG tetraloop taken from the structure deposited in the Protein Databank with the extension code 1F7Y.[7] The representation of the cUUCGg loop was produced with the program ViewerLite. clbp = closing base pair.

restrictions on the sequences that can be produced by in vitro transcription reactions. For an efficient transcription with T7-RNA-polymerase, the sequence should start with one or more guanine residues at the 5′ end.[15, 18] In addition, sequences shorter than ≈10 nucleotides are produced only very inefficiently. When linearized plasmids are used, the 3′-terminal nucleotide sequence should correspond to the recognition site of a restriction enzyme that allows linearization of the template. A further complication in the preparation of homogeneous RNA samples arises due to the fact that the T7-RNA-polymerase tends to add one or two additional nucleotides of random sequence that are not encoded by the template to the 3′ end of the transcript. The additional nucleotides give rise to inhomogeneous products of the transcription reaction, which lead to multiple sets of NMR resonances and complicate analysis of the spectra. To avoid this, the RNA can be transcribed as a fusion product with a cis-acting (intramolecularly acting) hammerhead ribozyme that self-cleaves cotranscriptionally[19, 20] to yield a uniform 3′ end with a 2′,3′-cyclic phosphate group.

For the purification of the desired RNA from nonincorporated nucleotides and abortive transcription products, preparative

 © 2003 Wiley-VCH Verlag GmbH & Co. KGaA, Weinheim

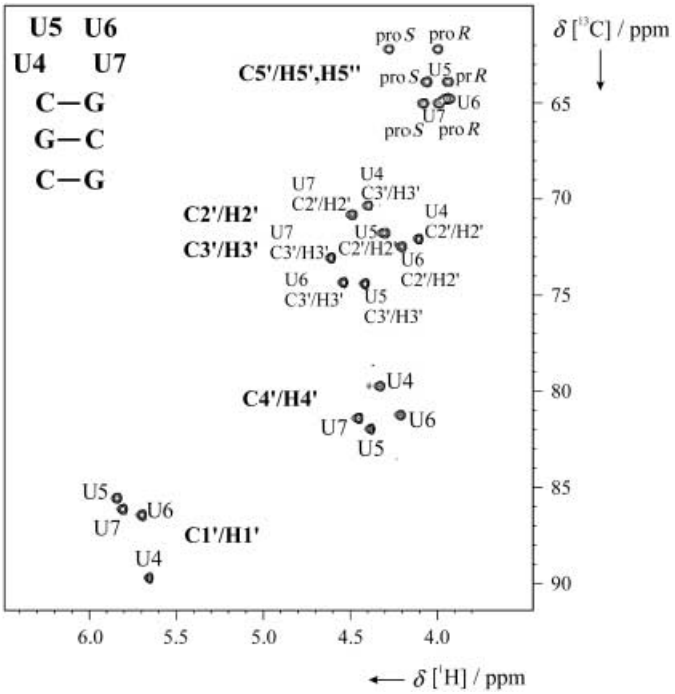

Figure 3. 2D $^{1}H,^{13}C$ correlation spectrum of the selectively ^{13}C-labeled 3'-CGC**UUUU**GCG-5' RNA. In this sample, only the ribose rings of four uracils are ^{13}C-labeled. This results in a considerable reduction of resonance overlap. If this spectrum were recorded on a larger RNA, for example, a 30-mer, and only four nucleotides were labeled, the chemical-shift resolution of all isotope-labeled residues would be retained.

polyacrylamide gel electrophoresis under denaturing conditions with gels containing 8 M urea is widely used. This method has the advantage that single nucleotide resolution can be achieved and the above-mentioned $n+1$ and $n+2$ products of the polymerase reaction can be separated. An alternative approach is the so-called 'ion-pair'-reversed phase HPLC.[21] Here, RNA complexed with the hydrophobic counterion tetrabutylammonium hydrogen sulphate is fractionated by increasing hydrophobicity by using an acetonitrile gradient.[22] The HPLC approach is especially efficient when preceded by an anion-exchange column step in which most of the unincorporated nucleotides and short abortive products can first be separated from the desired RNA product.[23] However, 'ion-pair'-reversed phase HPLC achieves single-nucleotide resolution only for oligonucleotides that have less than 20 residues. For longer RNA molecules, it is therefore advantageous to employ hammerhead ribozyme fusions since then essentially only two larger RNA molecules of different length need to be separated. Following the HPLC step, the fractions containing the desired RNA molecules are lyophilized and desalted on gel-filtration columns. The remaining tetrabutylammonium hydrogen sulphate can be separated from the RNA by precipitation with acetone/$LiClO_4$. Finally, the RNA has to be folded into a homogeneous form and exchanged into the buffer that will be used for NMR spectroscopy. Conditions for the correct folding of RNA have to be established individually for every new RNA molecule under study, therefore no general procedure can be given—especially for RNA molecules with more complex folds. However, simple hairpins can normally be obtained by a fast cooling step following a heat denaturation under conditions of low RNA and salt concentrations. High salt and RNA concentrations and slow cooling, on the other hand, favor the formation of duplex structures. A flow scheme for RNA preparation, as described in Stoldt et al.[23] and routinely used in our lab, is shown in Figure 5.

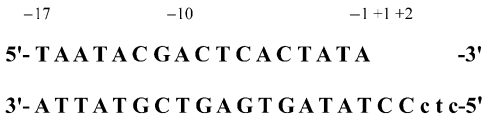

Figure 4. Consensus sequence of the T7-RNA-polymerase promoter. Nucleotides in positions +3 to +5 (lower case letters) can be chosen according to the sequence of the target RNA. Positions +1 and +2 should be guanine for efficient in vitro transcription.

3. Base-Pairing Pattern

3.1. Information about the base-pairing pattern from 1D NMR spectroscopy

Even in the early NMR studies of RNA molecules in the 1970s it was clear that the region of the imino proton resonances of the guanines and uracils between 10–15 ppm contained valuable information about base pairing in the RNA molecule. These signals are only observable when the imino protons are protected from exchange with the bulk solvent water and are therefore involved in hydrogen bonding. By counting the number of imino proton resonances, it is essentially possible

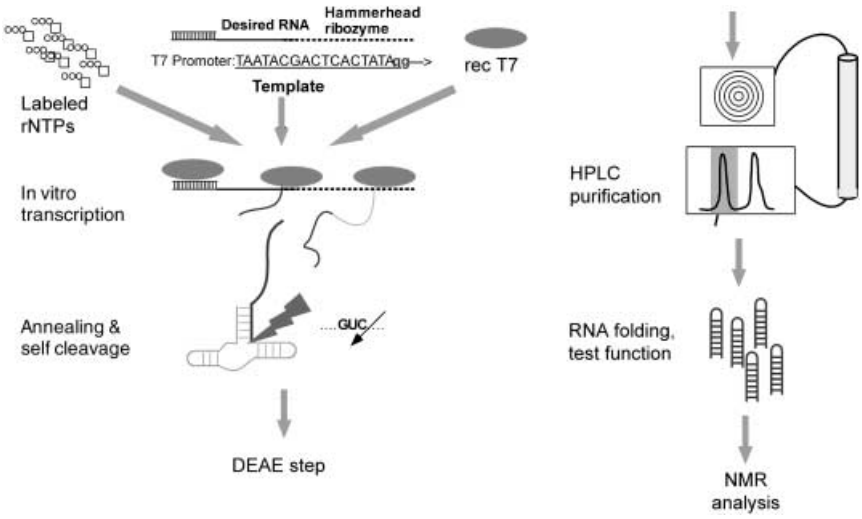

Figure 5. Flow scheme of the synthesis of isotope-labeled RNA molecules by in vitro transcription. For further explanations, see the text. DEAE = diethylaminoethyl, rec T7 = recombinant T7 polymerase, rNTPs = ribonucleotide triphosphates.

 © 2003 Wiley-VCH Verlag GmbH & Co. KGaA, Weinheim

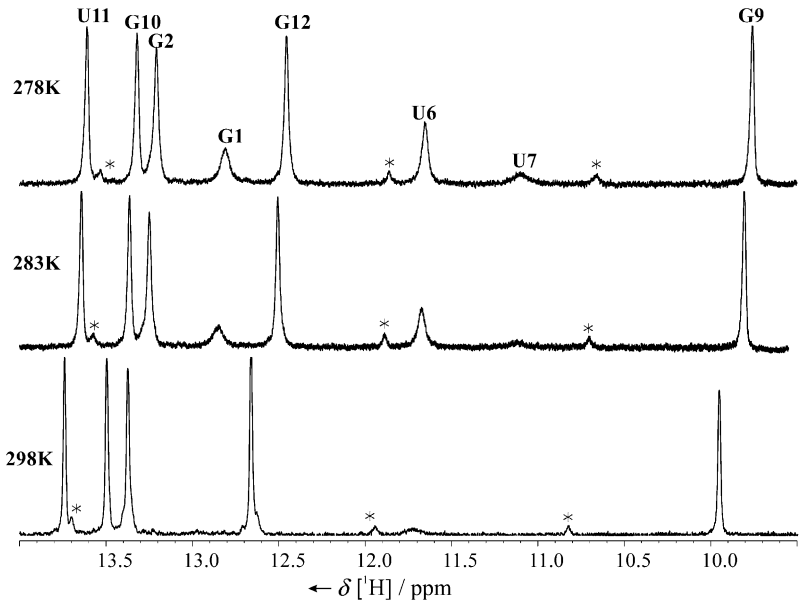

*Figure 6. Imino region of the 1D ^{1}H spectra of the 14-mer cUUCGg tetraloop RNA recorded at 600 MHz and three different temperatures (278, 283, and 298 K). Assignments are annotated for the imino proton resonances. Resonances stemming from the duplex form are indicated with *.*

correlates all protons within a distance of 5 Å. The chemical shifts of the imino proton resonances in RNA depend strongly on the chemical environment, on base stacking, on ring effects, and on hydrogen bonding to solvent molecules. The imino proton of guanine bases resonates at 12–13.5 ppm if it is involved in a G:C base pair and at 10–12 ppm if it is part of a G:U base pair (Table 1).[24, 25]

The traditional assignment strategy for base pairs is based on the observation of NOE contacts (as indicated in Figure 7). A:U base pairs are easily identified by a strong NOE cross-peak between the H2 proton of adenine and the uracil H3 imino proton. In G:C base pairs, the H1 imino proton of guanine shows a strong NOE contact to the amino protons of the base-pairing cytosine. For this reason, the amino protons of cytosines involved in base pairing are easy to identify in comparison to the guanine and adenine amino protons. In ^{13}C- and ^{15}N-labeled RNA molecules, identification of the cytosine amino protons can be used for further correlation to the H5 and H6 aromatic protons by direct correlation experiments (see Section 6). In helical RNA, NOESY cross-peaks can be observed between guanine H1 imino protons and cytosine H5 protons due to spin diffusion. Typical NOE interactions are shown in Table 2.

Imino–imino NOE cross-signals occur sequentially and between strands. As a consequence, there is no differentiation between sequential intra- and intercatenar NOE contacts. Chemical-shift information about imino protons can be helpful

to count the number of base pairs. In addition, imino protons of Watson–Crick base pairs tend to be found in the region of 12–15 ppm, whereas imino protons of noncanonical base pairs often have upfield chemical shifts (Figure 6). The stability of RNA molecules can be investigated by following temperature-induced changes in the 1D imino spectra.

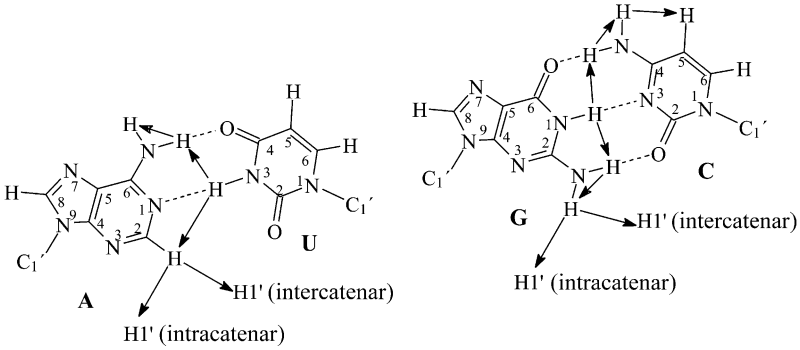

Figure 7. Schematic representation of the Watson–Crick base pairs A:U and G:C. The arrows indicate possible NOE contacts.

3.2. Information about base pairing from homonuclear 2D NOESY experiments: Sequential assignment of imino proton resonances

The starting point for the determination of the hydrogen-bonding pattern is to sequentially assign the well-resolved resonances of the imino protons in a 2D NOESY experiment. As depicted later, the NOESY experiment

Table 1. Chemical shifts (δ) of imino and amino resonances in Watson–Crick base pairs and wobble base pairs.

Base pair	Base-pair atoms	Chemical-shift regions [ppm]	Distance [Å]
G:C	G N1–H1 ··· N3 C	12–13.5	1.89
	G N2–H2 ··· O2 C	8–9	2.08
	G O2 ··· H4–N4 C	8-9	1.71
	G N2–H2	6.5–7	–
	C N4–H4	6.5–7	–
U:A	U N3–H3 ··· N1 A	13–15	1.93
	U O4 ··· H6–N6 A	7.5–8.5	1.82
	A N6–H6	6.5–7	–
G:U	G N1–H1 ··· O2(O4) U	10–12	1.76
	G O2 ··· H3–N3 U	11–12	1.96

Table 2. NOE cross-peaks that are usually observed in a helical region of RNA.

NOE correlation	Sequential	Intrabase pair
NH–NH	weak	strong (only G:U)
NH–H_2	weak	strong
NH–NH_2	weak	strong
NH_2–NH_2	weak	–

 © 2003 Wiley-VCH Verlag GmbH & Co. KGaA, Weinheim

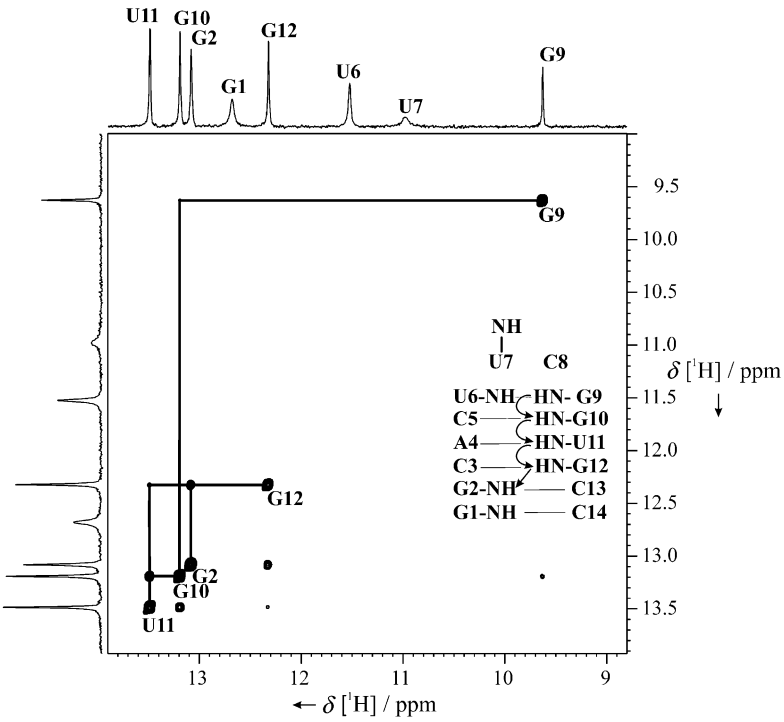

Figure 8. The imino – imino proton cross-peak region of the cUUCGg tetraloop in a 2D NOESY spectrum at 700 MHz with excitation sculpting for water suppression. The lines indicate the imino proton connectivity. The insert shows the sequence with the imino protons and the arrows indicate the sequential assignment walk. The NOESY mixing time was 300ms at 298K. As a result of exchange with the solvent, both cross-peaks and diagonal peaks of guanine 1, uridine 6, and uridine 7 are absent.

in the assignment of the NOESY signals (Table 1). In the $cU^6U^7C^8G^9g$ tetraloop, the imino proton of G9, which resonates at 9.6 ppm, serves as a starting point for the assignment of the imino proton region of the NOESY experiment (Figure 8). The sequential NOE contacts can easily be assigned following the primary sequence of the cUUCGg tetraloop. In the tetraloop, the stability of the G:U base pair differs from that of the G:C base pairs. The expected NOE cross-signal to U6, which is involved in a U6:G9 base pair, is not visible due to fast water exchange of the imino proton of U6; this is also the reason for the absence of diagonal peaks for the nucleotides G1 and U7. The water exchange is also responsible for the apparent asymmetry of the cross-peak intensities of the NOESY spectrum.

By using NOE information, it is therefore possible to distinguish Watson – Crick G:C and A:U base pairs. Stable G:U wobble base pairs can be identified by a strong NOE contact between the guanine imino and uracil imino protons. Furthermore, NOE contacts between the imino protons of neighboring base pairs are observable and facilitate the sequential assignment of the imino proton signals (Table 2). With this information, it has been possible to derive secondary structure models of tRNA molecules[26–28] and 5S rRNA.[29–31]

3.3. Information from heteronuclear 2D HSQC and HNN-COSY experiments: Elucidation of base pairing and secondary structure

With the introduction of ^{15}N-labeling and heteronuclear correlation experiments it becomes easier to distinguish between uracil and guanine imino resonances since the resonance frequencies of the imino nitrogen atoms are separated by ~10 ppm (Table 3; Figures 9 and 10). However, a major breakthrough for the elucidation of base-pairing and more complex hydrogen-bonding patterns in RNA by NMR spectroscopy was the discovery that sizeable scalar couplings across an N–H···N-type hydrogen bond can be observed between the nitrogen atom and proton of the hydrogen-bond donor and the nitrogen atom of the hydrogen-bond acceptor [32, 33] in RNA and DNA through the use of a so-called HNN-COSY experiment.

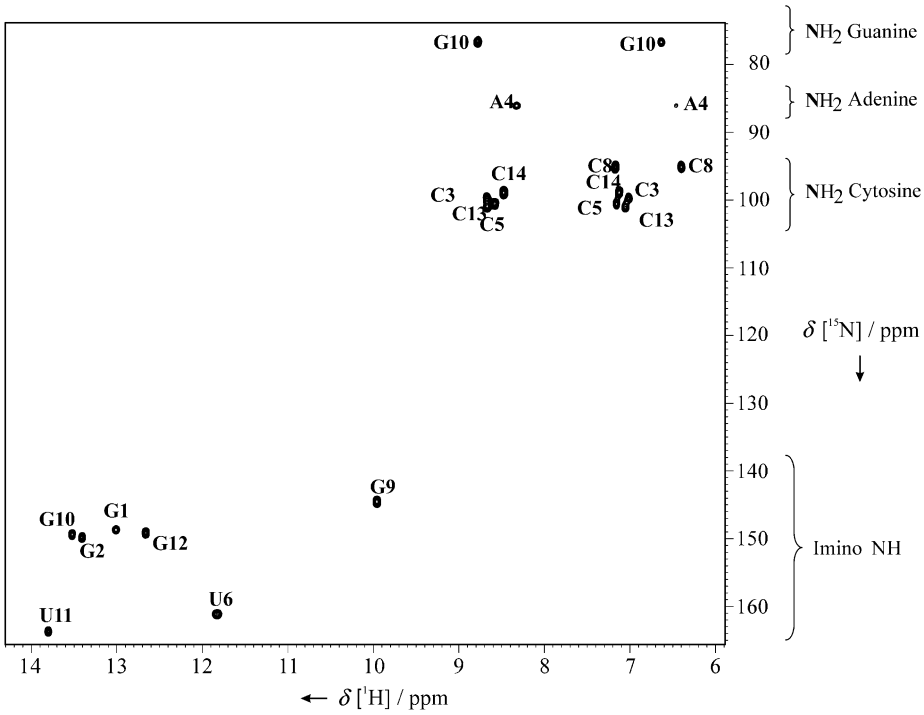

Figure 9. ^{1}H,^{15}N-HSQC spectrum of the cUUCGg tetraloop at 700 MHz recorded at 283 K. The assignment is indicated.

 © 2003 Wiley-VCH Verlag GmbH & Co. KGaA, Weinheim

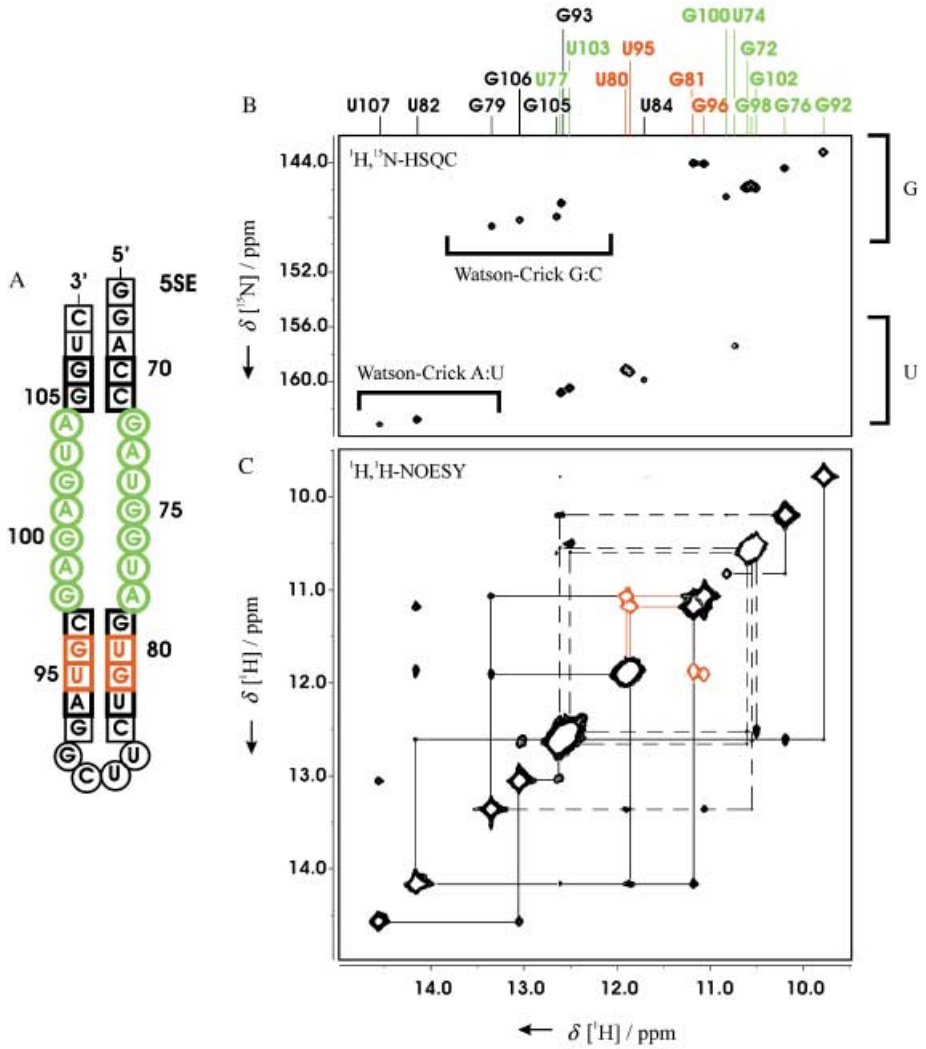

Figure 10. *Example of secondary structure determination for longer RNA molecules based on imino group signals. A) Secondary structure of an RNA hairpin containing nucleotides 70 – 82 and 94 – 106 of E. coli 5S rRNA, the so-called E-loop. B) Imino group region of the ^{15}N,^{1}H-HSQC spectrum with the assignments of the proton resonances given at the top. Imino groups of noncanonical base pairs are shown in green, imino groups of wobble G:U base pairs are indicated in red, and imino groups of Watson – Crick base pairs are depicted in black. The ^{15}N-chemical-shift ranges for G and U imino groups, respectively, are indicated on the right of the spectrum. The typical ^{1}H-chemical-shift ranges for imino groups in Watson – Crick base pairs are indicated as well. C) Sequential assignments of imino resonances by sequential NOE contacts. Solid and dashed lines indicate sequential NOE interactions for the 5′ and the 3′ halves of the molecule, respectively. Intra-base-pair NOE contacts between G and U imino resonances typical for stable wobble G:U base pairs are marked with red lines.*

Table 3. *Chemical shifts (δ) of resonances observed in ^{1}H,^{15}N-HSQC and ^{1}H,^{13}C-HSQC spectra.*

Atoms	δ^1H [ppm]	δ^{15}N [ppm]	δ^{13}C [ppm]
C1′H1′	4.4 – 6.5	–	89 – 95
C2′H2′	4-5	–	70 – 80
C3′H3′	3.8 – 5	–	70 – 80
C4′H4′	3.8 – 4.8	–	81 – 86
C5′H5′	2.5 – 5	–	62 – 70
C2H2	6.5 – 8.5	–	150 – 154
C5H5	5.0 – 6.3	–	167 – 170
C6H6	7.0 – 7.7	–	137 – 140
C8H8	7.0 – 8.0	–	133 – 140
NH_2 (amino)	6.5 – 9.0	74 – 76 G	–
		80 – 82 A	–
		96 – 98 C	–
NH (imino)	9.0 – 15	145 – 148 G	–
		157 – 162 U	–

The HNN-COSY experiment utilizes the through-space scalar ^{2h}J(N,N) coupling constant in base pairs of RNA and DNA, which monitors the interaction from ^{15}N imino donor nuclei and the corresponding ^{15}N acceptor nuclei of the complementary bases. The ^{2h}J(N,N) coupling constants between N3 of uracil and N1 of adenine as well as between N1 of guanine and N3 of cytosine are of the order of 5 – 7 Hz. During the pulse sequence, which is a straightforward extension of the HNHA experiment by Vuister and Bax,[34] one part of the originally generated magnetization remains on the starting nitrogen atom (annotated DP in Figure 11), whereas the other part is transferred to the hydrogen-bonded nitrogen atom (annotated CP in Figure 11). This gives rise to a diagonal peak and a cross-peak at the ^{15}N frequency of N1 of guanine and N3 of cytosine. Due to a modulation of both peaks by either $\sin^2(^{2h}J(N,N)T)$ or $\cos^2(^{2h}J(N,N)T)$, the size of the coupling constant can be obtained by comparing the peak volumes I^{cross} and I^{diag} of the cross-signal to the diagonal signal ($I^{cross}/I^{diag} = \tan^2(2\pi\ ^{2h}J(N,N)T)$).

 © 2003 Wiley-VCH Verlag GmbH & Co. KGaA, Weinheim

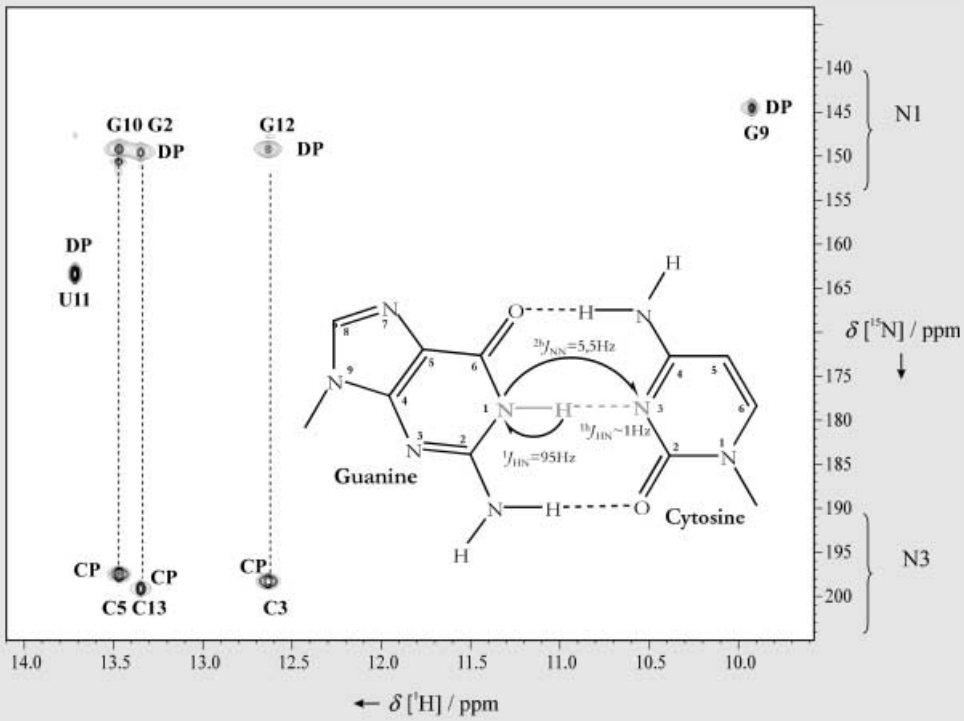

Figure 11. HNN-COSY experiment at 700 MHz and 298 K. On the right side, a Watson – Crick G:C base pair is depicted. The coupling constants are annotated. In this experiment, N1 of guanine can be correlated with the quaternary nitrogen atom of the cytosine residue.

It quickly became clear that similar scalar couplings could be observed for N–H···N-type hydrogen bonds in noncanonical base pairs as well. Remarkably, since the chemical shifts of the different possible nitrogen donor and acceptor groups are well separated, it is often possible to directly derive the base-pairing pattern. Thus, by using the cross-hydrogen-bond scalar couplings it was possible to characterize base pairing in A:A, G:A (see Figure 12), and G:G mismatches (for examples, see refs. [35 – 38]), reversed Hoogsteen A:U base pairs,[38] Watson – Crick-type U:C base pairs,[39] and base-triples[40, 41] in DNA, RNA, and RNA – protein complexes. Even intermolecular hydrogen bonds between guanine N7 nitrogen atoms and arginine side-chain guanidinium groups in an RNA – peptide complex could be detected.[42] This experiment can also be applied to A:U base pairs when D_2O is the solvent.[40, 43, 44] The correlation starts on the H2 proton of adenine and the magnetization is transferred to N1 of adenine (^2J(H2,N1) = 14.5 Hz) and to the hydrogen-bonded N3 of uracil. By direct observation of the hydrogen bond in D_2O, it is possible to differentiate between Watson – Crick and Hoogsteen base pairs.

Scalar couplings across hydrogen bonds can be observed for N–H···O=C-type hydrogen bonds as well, at least in small nucleic acids.[45][42] However, there the coupling constants are much smaller than that of the N–H···N-type hydrogen bonds, which makes their direct detection by NMR spectroscopy much harder. Only recently, it was found that tertiary hydrogen bonds between a 2′-hydroxy group as the hydrogen-bond donor and a nitrogen atom as the acceptor also give rise to measurable scalar couplings.[46]

The elucidation of hydrogen-bonding patterns involving carbonyl groups as acceptors might also benefit from chemical-shift analysis. In particular, the chemical shifts of the C2 and C4 carbonyl groups of uracils that can be measured in ^{13}C-labeled RNA molecules are influenced by their involvement in hydrogen bonds. Thus, when comparing the chemical shifts of uracil C4 and C2 groups in Watson – Crick A:U base pairs, in which C4 is a hydrogen-bond acceptor and C2 is not hydrogen bonded, with those in a wobble G:U base pair, where C2 is hydrogen bonded and C4 is not, the signal for C4 in the A:U base pair is shifted downfield with regard to that for C4 in the G:U base pair, whereas the signal for C2 in the A:U base pair is shifted upfield. Interestingly, in reversed Hoogsteen A:U base pairs, where C2 of uracil is the hydrogen-bond acceptor in contrast to C4 in a Watson – Crick A:U base pair, the C2 chemical shift is comparable with that in a wobble G:U base pair (Wöhnert, unpublished results). This relationship holds true for U:U base pairs as well. For instance, in asymmetric U:U base pairs, two N–H···O=C hydrogen bonds are observed, one with C2 as the acceptor and one with C4 as the acceptor. Accordingly, one C4 group and the C2 group of the other uracil are not involved in a hydrogen bond. For one uracil in the base pair, a downfield-shifted C4 signal and an upfield-shifted C2 signal are observed, whereas for the other uracil the C4 signal is shifted upfield and the C2 signal is shifted downfield (Figure 13).[47][39] However, these chemical-shift signatures of carbonyl groups must be further explored in other base-pairing geometries, before they will become a general tool for the assignment of hydrogen-bonding patterns.

4. Description of a Hairpin – Duplex Equilibrium with NMR Spectroscopy

Secondary structure formation in RNA molecules depends on many factors, for example, sample concentration, salt concentration, pH value, and temperature. In the optimization of the formation of one specific conformation, monitoring of the imino region in a proton 1D NMR experiment proves helpful. As an example, we show the results for a cUUUUg tetraloop (5′-CGCUUUUGCG-3′; Figure 14). Similarly to UUU loops[22] the cUUUUg tetraloops can form a hairpin and a duplex; at elevated temperature, the hairpin melts to form single-stranded RNA (Figure 14 E).[48] We start with low sample concentration (0.15 mM) and change both the phosphate and NaCl concen-

 © 2003 Wiley-VCH Verlag GmbH & Co. KGaA, Weinheim

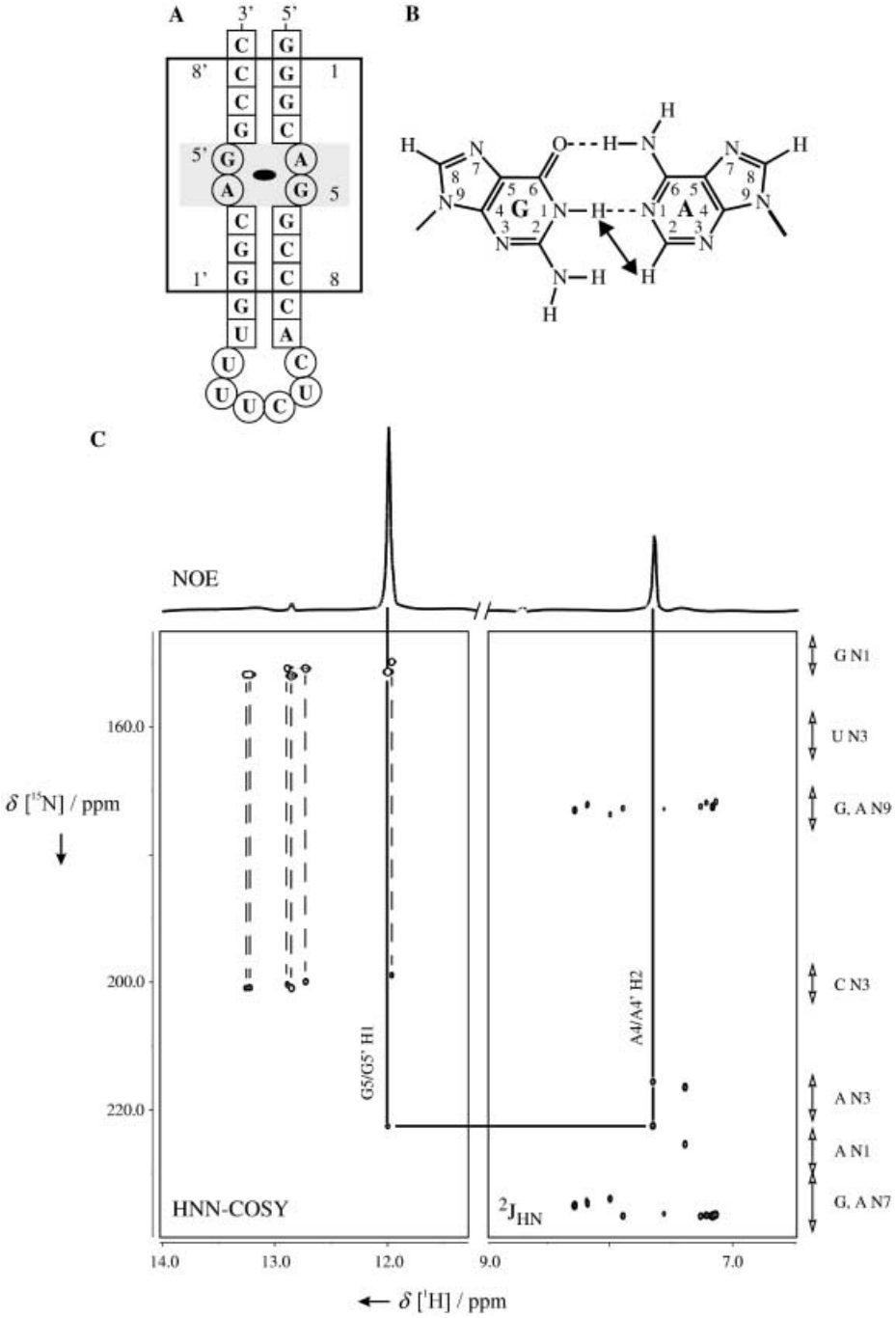

Figure 12. Identification of an imino-hydrogen-bonded G:A base pair with a G N1H1 – A N1 hydrogen bond in the HNN-COSY experiment. A) Secondary structure of an RNA hairpin with a tandem G:A mismatch with a pseudo twofold symmetry. B) Geometry of an imino-hydrogen-bonded G:A base pair. An expected strong NOE contact between the G imino proton and the A H2 proton typical for this base-pairing geometry is indicated by an arrow. C) Identification of the donor and acceptor groups involved in the hydrogen bond by a combination of the HNN-COSY, $^2J_{HN}$-^{1}H,^{15}N-HSQC, and NOESY spectra. The HNN-COSY spectrum shows cross-correlations between G H1 hydrogen atoms and G N1 and C N3 nitrogen atoms (dashed lines) typical for Watson – Crick G:C base pairs and between the G5/G5′ H1 hydrogen atom and the G5/G5′ N1 and A4/A4′ N1 nitrogen atoms (solid line). The assignment of the nitrogen atom as an adenine N1 is supported by the $^2J_{HN}$-^{1}H,^{15}N-HSQC spectrum, which provides a correlation from the A4/A4′ H2 hydrogen atom to the A4/A4′ N1 and N3 nitrogen atoms (solid line). Typical chemical-shift ranges of the relevant nitrogen atoms are indicated at the right side of the spectrum. A one-dimensional cross-section from a 2D ^{1}H,^{1}H-NOESY spectrum taken at the chemical shift of the G5/G5′ H1 hydrogen atom shows the expected strong NOE cross-peak to the A4/A4′ H2 hydrogen atom.

trations (Figure 14 A). The phosphate concentration has only a small effect on the line shape of the resonances. In contrast, increasing the NaCl concentration has a pronounced effect on the line shape and the chemical shift of resonances in the spectra. The signals at 12.5 – 13 ppm are guanine imino protons and the signals at 10.5 – 11.5 ppm are uracil imino protons. The upfield shift of the uracil resonances is unusual and results from U:U base pairs. When the concentrations of RNA and NaCl are increased (120 mM), four sharp lines appear, which arise from the formation of two U:U base pairs in the duplex conformation (Figure 14 B). The temperature dependence of the NMR spectra reveals that the duplex conformation is only stable at low temperature (3 °C; Figure 14 C). At 27 °C, only the hairpin conformation is visible, and at even higher temperatures, the hairpin melts, the exchangeable resonances disappear, and the aromatic signals resonate at positions characteristic for single-stranded RNA. The temperature transitions are reversible and are also evidenced in native gels (Figure 14 F, G). The 2D NOESY spectra of the uracil imino signals provide clear evidence that all four uracils form base pairs to each other (Figure 14 D).

Such transitions of secondary structure are also observed for other RNA molecules.[49] The D-loop of *Escherichia coli* 5S rRNA, for example, can exist as both a stem-loop and as a duplex with two U:U base pairs in the bulge region. Additionally, only the dimeric form can be observed in crystals of the RNA molecule. Since there is only a slow interconversion of the conformations in solution, NMR spectroscopy can be used as a tool for screening of the best crystallization conditions to get crystals containing exclusively the monomeric or dimeric form of the RNA molecule.

To distinguish between either duplex RNA or RNA hairpins, pulse-field-gradient NMR experiments[50, 51] can be used to measure diffusion con-

 © 2003 Wiley-VCH Verlag GmbH & Co. KGaA, Weinheim

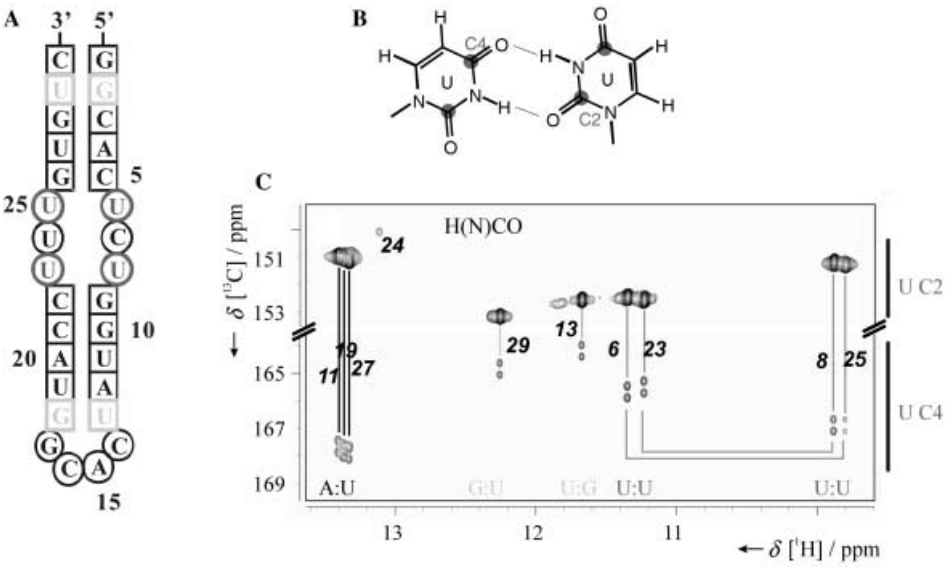

Figure 13. Chemical-shift dependence of the uracil C2 and C4 chemical shifts on base pairing. A) Secondary structure of an RNA hairpin containing A:U, wobble G:U, and asymmetric U:U base pairs. B) Geometry of an asymmetric U:U base pair. For one of the uracils C2 is the hydrogen-bond acceptor as in a wobble G:U base pair, whereas in the other one C4 is the hydrogen-bond acceptor similar to an A:U base pair. C) H(N)CO spectrum of the hairpin RNA. The chemical-shift ranges for the C2 and C4 carbons are indicated.

stants.[52] Due to the dependence on both the length and the shape of the RNA molecule, the diffusion constant proves to be a sensitive measure of both forms of an RNA molecule.

5. Elucidation of RNA – Metal-Ion Interactions

It has long been known that for many RNA molecules, metal ions are integral parts of their tertiary structure. This idea has recently been extended towards the notion that complex RNA tertiary structures possess a metal-ion core analogous to the hydrophobic core in protein structures.[53] Thus, it is not surprising that many RNA molecules contain specific binding sites for monovalent and divalent metal ions. NMR spectroscopic approaches to characterize metal-ion binding are based either on chemical-shift changes, paramagnetic line broadening, or intermolecular NOE contacts.

Chemical-shift changes can be measured with any ion. The chemical-shift changes induced by ion binding can be either directly transmitted due to the deshielding effect of the ion or due to an ion-induced structural transition of the RNA. For instance, chemical-shift changes induced by high concentrations of sodium, magnesium, and lead ions have been used to map out metal binding sites for the lead-dependent ribozyme.[54] Butcher et al.[55] used magnesium ions and cobalt hexamine ions to identify metal binding sites in the two domains of the hairpin ribozyme. In both ribozymes, it was found that the metal binding site is preformed in the RNA structure. Cobalt hexamine is an analogue of a hexahydrated magnesium ion but causes larger chemical-shift effects due to its higher charge. It has been introduced by Kieft and Tinoco as a mimic of outer-sphere complexation of hydrated magnesium ions by RNA.[56] Sensitive reporters of chemical-shift changes induced by metal-ion binding are not only the resonances of the proton, nitrogen, and carbon nuclei of RNA but also the phosphorus resonances as part of the negatively charged RNA backbone. By using ^{31}P chemical-shift changes upon addition of magnesium, Hansen et al.[57] identified a high-affinity Mg^{2+} binding site in the catalytic core of the hammerhead ribozyme that was not found in the published crystal structure. Butcher and co-workers[58] added an interesting new twist to this approach. In their investigation of a core component of the spliceosome, the U6 RNA intramolecular stem-loop, they inserted a single thiophosphate group into the backbone of the molecule and measured the chemical-shift changes induced by the thiophilic cadmium ion. Interestingly, they could show that cadmium bound with high diastereoselectivity when the pro *S* but not the pro *R* oxygen atom was replaced with a sulfur atom.

Chemical-shift mapping as a probe for magnesium binding sites is often complemented by paramagnetic line-broadening studies, where the paramagnetic manganese ion is used to replace magnesium.[59] The presence of the paramagnetic ion results in an enhanced relaxation of the nuclei in its vicinity and in turn leads to the disappearance of their NMR signals. The strength of the effect is dependent on the distance and can therefore be used to extract distance information that can be incorporated in the structure calculation of the ion – RNA complex.[55]

However, a more direct way to obtain distance information is to use intermolecular NOE contacts. These become available when cobalt hexamine is used as a mimic of magnesium[56] or ammonium ions are used to mimic monovalent cations such as potassium or sodium.[55] By using intermolecular NOE contacts between the amino groups of the complex ion and the RNA protons, the Tinoco group solved the structures of cobalt hexamine bound to domains of the group 1 intron,[56, 60] a frameshifting pseudoknot of the mouse mammary tumor virus,[61] the GAAA stable tetraloop,[62] and the P4 element of the RNase P ribozyme.[63] In many cases, the metal binding pocket was formed by tandem mismatch base pairs, such as tandem G:U base pairs[60] and tandem G:A base pairs.[62]

6. NMR Resonance Assignment of RNA

The first step for a complete resonance assignment is the identification of nucleobase spin systems (H^N, NH_2, H2, H5, H6, and H8). Secondly, the protons of the sugar moiety (H1′, H2′, H3′,

 © 2003 Wiley-VCH Verlag GmbH & Co. KGaA, Weinheim

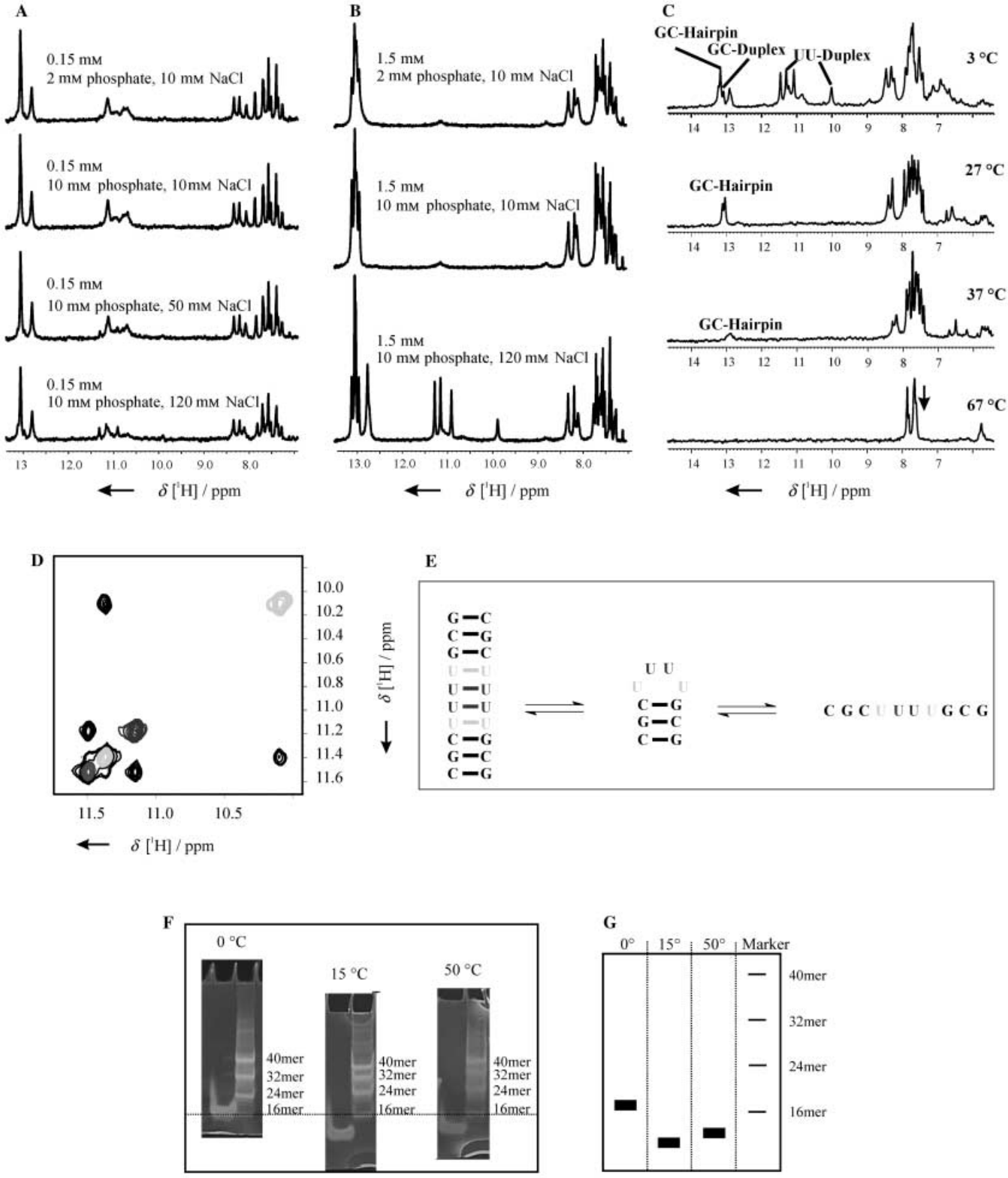

Figure 14. *1D JR-Echo spectra at 600 MHz on the cUUUUg loop RNA. A) With different salt concentrations and 0.15 mM RNA at 7°C. B) With different salt concentrations and 1.5 mM RNA at 7°C. C) With a 1.5 mM RNA sample at different temperatures. D) The 2D imino proton NOESY spectrum for the U duplex cross-peaks. The indicated black and grey cross-signals belong together to one base pair. E) Schematic representation of the temperature-induced conformational change. F) The native gels of the cUUUUg tetraloop RNA at three different temperatures with a DNA marker. The gels were calibrated on the lane of the DNA 16 mer for better comparison. G) Schematic representation of the native polyacrylamide gels.*

 © 2003 Wiley-VCH Verlag GmbH & Co. KGaA, Weinheim

H4′, H5′, H5′′) are assigned. The spin systems of the nucleobases are correlated with the sugar spin system either by observation of NOE contacts between aromatic and H1′ protons or by direct correlation of the H1′ resonances with the resonances of the glycosidic nitrogen atoms of the nucleobases in HCN-type experiments. As a third step, the assignments for the ribose spin systems are completed by optimized HCCH-TOCSY experiments. Then, sequential links between the nucleotide spin systems are established by sequential NOE experiments (H6/H8 to H1′) or by HCP and HCP-TOCSY experiments. In these four steps, a complete assignment of all atoms can be established.

6.1 Assignment of the aromatic protons of the nucleobases: Correlation of imino to aromatic protons

Traditionally, aromatic protons in pyrimidines of RNA are assigned by examining NOE cross-signals from imino protons to the H5 proton of cytosine and uracil. By using long mixing times, cross-peaks to H6 are also observed due to spin diffusion. Unfortunately, there is no direct solution for assigning H8 of guanine and adenine. In uniformly ^{13}C- and ^{15}N-labeled RNA molecules, a direct correlation of H8 resonances with N7 and N9 nitrogen by using ^{n}J coupling constants is possible. The different transfer pathways of the available pulse sequences are summarized in Figure 15.

The first experiments to correlate hydrogen atoms from the Watson–Crick site of the nucleobase to the hydrogen atoms H8 (purines) and H6/H5 (pyrimidines) were developed by Simorre et al.,[64, 65] Sklenar et al.,[66] and Fiala et al.[67] Simorre et al.[65] (Figure 15 A) introduced a pulse sequence that was specific for guanine nucleotides. From the imino proton, the magnetization is transferred through an INEPT step to N1. By using CN-TOCSY transfer (DIPSI-3, field strength 1.9 kHz), the magnetization is transferred to the base carbon C6. The ^{15}N and ^{13}C carriers are set to 146 ppm and 161 ppm. The homonuclear TOCSY-period (FLOPSY-8) with a duration of 38 ms and an rf field strength of 5 kHz transfers the magnetization directly to C8 or through C6 and C4 to C8. For this step, the carrier is set to 145 ppm. Subsequently, the in-phase C8 coherence is transferred by reverse refocused INEPT steps to H8.

In Figure 15 D, E, the transfer pathways exploited in the experiment reported by Sklenar et al.[66] are depicted: the magnetization is transferred in a reverse manner from H8/H6 to the imino proton. For the CC transfer and the CN transfer the same rf field strength of 2.9 kHz is applied. Mixing times for CC-TOCSY and CN-TOCSY transfer are 19 ms and 58 ms, respectively. The carrier is set to 150 ppm for ^{13}C and 153 ppm for ^{15}N. This pulse sequence is also applicable to guanine and uracil bases.

The pulse sequence by Fiala et al.[67](transfer pathway in Figure 15 D) correlates the nonexchangeable protons with the exchangeable protons in guanine bases. The CN transfer is achieved by INEPT steps with a selective C6 pulse. The carrier for ^{15}N is set to 120 ppm, which corresponds to the middle of the resonance frequency of N1 and NH_2. The CC-TOCSY mixing time is 55 ms with a field strength of 3 kHz on carrier at 150 ppm.

All three experiments are quite similar; the main difference is the TOCSY transfer step and the chosen carrier frequency. Also the last experiment uses a CN-INEPT instead of CN-TOCSY. Wijmenga and van Buren[2] simulated the transfer efficiency of these sequences. The efficiency depends only on the CC-TOCSY step. CN-INEPT and CN-TOCSY transfer steps are equal in their transfer efficiencies. The simulation shows that the main transfer is supplied by the C8–C6 route and indicates that the sequence by Simorre et al. is the most efficient for larger systems. The sequence by Sklenar et al. has the advantage that it correlates imino protons in guanines and in uracils with nonexchangeable protons in a single experiment; the disadvantage is that it shows the worst transfer efficiency as compared to the other sequences. However, for RNA molecules which give rise to high-quality NMR spectra, the desired correlation peaks can be observed, as shown in Figure 16 where the sequence was applied to the cUUCGg tetraloop RNA.

A second pulse sequence by Simorre et al.[64] (Figure 15 B, C) correlates the exchangeable protons in uracil (H3) and guanine (NH_2) with the H6 protons. In this experiment, the magnetization is transferred from C4 to C6 not by a CC-TOCSY step but by using two INEPT transfers because of the different chemical shifts and coupling constants of C4, C5, and C6.

The correlation of the H2 protons with the H8 protons can be achieved in an HCCH-TOCSY experiment[68, 69] (Figure 15 F). The carbon network in

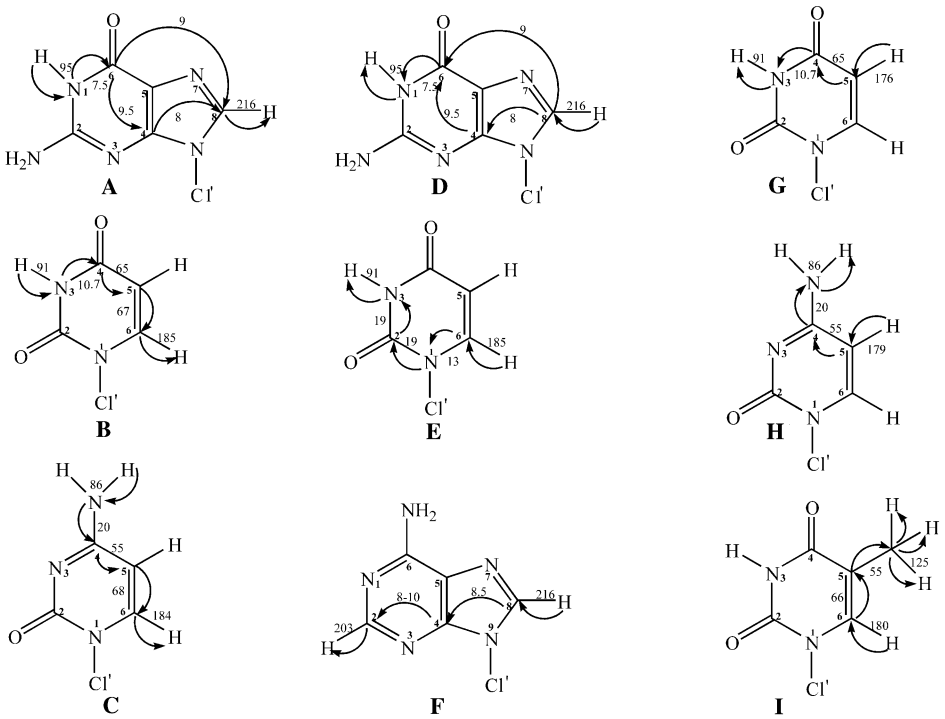

Figure 15. The transfer ways for the NMR experiments correlating nuclei in the nucleobases: A) HNC-TOCSY-CH, B) and C) HNCCCH, D) and E) HCCNH TOCSY, F) HCCH TOCSY, G) and H) H5(C5C4N)H, and I) H6C6CCH$^{(Me)}$. References are given in the text, numbers on the arrows indicate the size of scalar couplings between the connected atoms in Hz.

 © 2003 Wiley-VCH Verlag GmbH & Co. KGaA, Weinheim

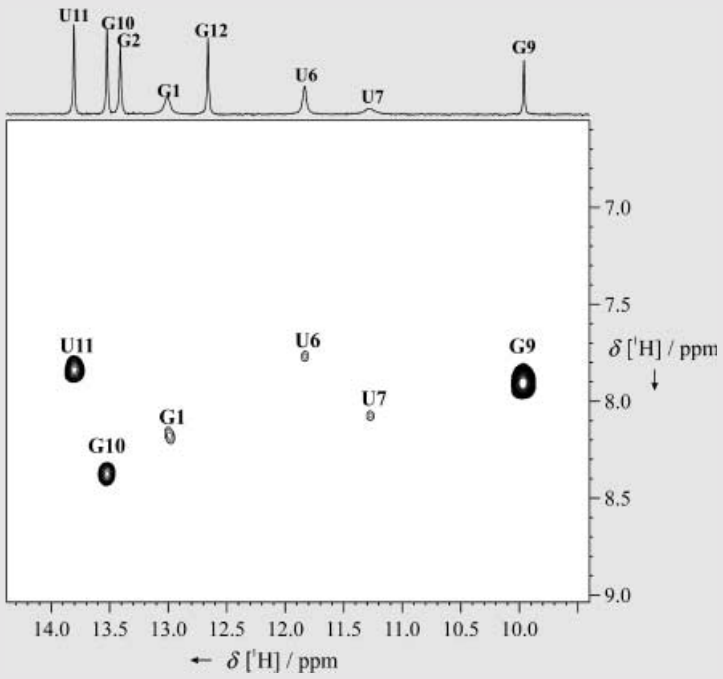

Figure 16. 2D HCCNH experiment (Sklenar et al.[66]) on the cUUCGg tetraloop RNA at 700 MHz.

adenine is relatively complex and with a CC-TOCSY experiment a considerable part of the magnetization is lost through unwanted coherence transfer pathways (for example, involving the spin of C5). An alternative way to achieve this correlation is the HMBC experiment.[70]

Wöhnert et al.[71] (Figure 15 G, H) correlated the H5 proton in uracil and cytosine with the exchangeable protons by applying sequential relay steps with selective pulses. For ^{13}C-labeled DNA, it is possible to correlate the H6 proton with the methyl group in thymine nucleotides[72] (Figure 15 I).

Recently, a modified pulse sequence has been developed by Wöhnert et al.[73] for the simultaneous correlation of either H6/H5 or C5/C6 to exchangeable protons in pyrimidines. The experiment uses the same transfer pathway depicted in Figure 15 B, C but in the opposite direction, starting from the nonexchangeable protons. This experiment has a high sensitivity.

6.2 Assignment of protons of the sugar moiety: Correlation of aromatic protons to sugar protons

Interresidual sequential assignment in helical A-form RNA is obtained by observation of NOE contacts between aromatic and sugar protons (Figure 17). All aromatic protons show NOE cross-peaks to the H1′ protons of their own ribose and to the preceding nucleotide in the 5′ direction. Although the sequential H1′ aromatic proton distance is larger than 4 Å in helical A-form RNA, a cross-peak can be observed due to spin diffusion through the H2′ proton.[74] The major problem in applying this NOE-based assignment procedure is to find suitable starting or anchoring points for the assignment walk. One possibility is to use the H2 protons of adenine. The distance between H2 and the sequential H1′ proton in helical A-form RNA is shorter than 4 Å. The H2 proton can be identified by NOE contacts to the uracil imino proton in H_2O or in a ^{1}H,^{13}C-HSQC, because the C2H2 region (150 ppm) is well resolved and no signals arising from other resonances are observed.

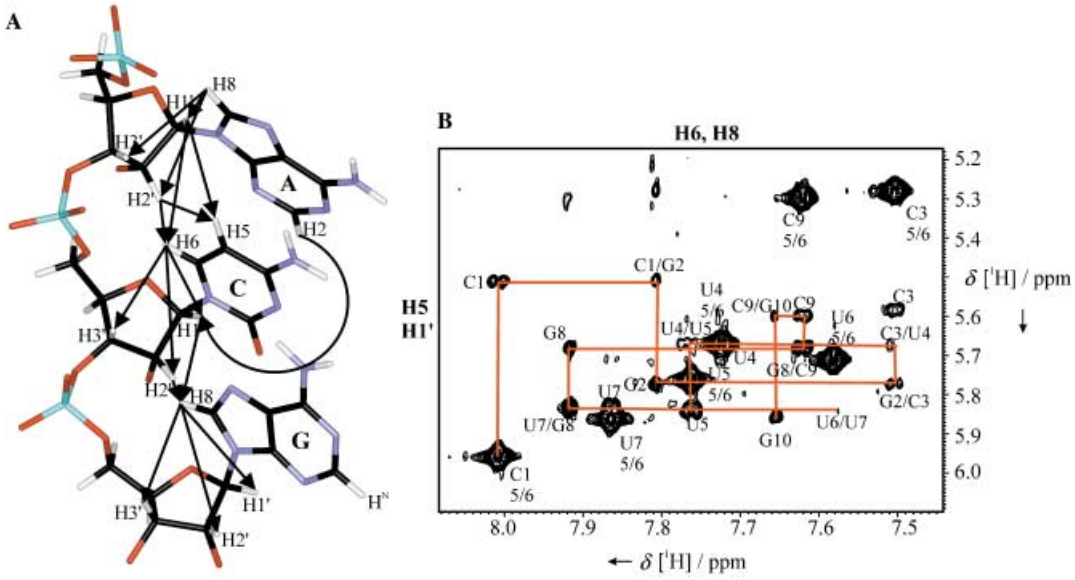

Figure 17. A) Schematic representation of the sequential assignment strategy in helical A-form RNA for nonexchangeable protons. The arrows show the intraresidual NOE connectivities between the aromatic and the sugar protons H1′ – H3′ and the sequential NOE correlation between the H3′ – H6, H8 protons and the H5 – H1′ protons. The sequential assignment of the helical A-form conformation is possible by determination of these NOE cross-peaks. In addition to the exchangeable protons, only the intercatenar NOE interactions between the adenine H2 and H1′ of the corresponding RNA strand give information about the helical conformation. B) An example for the NOESY assignment procedure shown for the cUUUUg loop RNA. The NOESY spectrum was recorded in D_2O at 600 MHz and the mixing time was 300 ms. Annotation by using two residues indicates connectivities due to sequential NOE contacts and annotation with one nucleotide indicates intraresidual NOE interactions.

 © 2003 Wiley-VCH Verlag GmbH & Co. KGaA, Weinheim

The NOE cross-peaks of 5′- and/or 3′-terminal nucleotides can serve as alternative starting points. The chemical shifts of the protons in terminal nucleotides are shifted, for example, the chemical shifts of H2′ and H3′ protons at the 3′ end are moved lower field because of the missing phosphate group.

In A-form helices, three relatively strong NOE contacts and one weak NOE are observed for every aromatic proton in the aromatic – sugar region in the NOESY spectra recorded with short mixing times (50 – 100 ms; Table 4). Strong NOE contacts reveal inter- and intranucleotide connectivities to the H3′ proton (distances smaller than about 3 Å) and a very strong NOE exists to the sequential H2′ proton (distance about 2 Å). The intra-residual aromatic/H2′ cross-peak is weak. These strong NOE contacts to the neighboring nucleotides arise due to intra-catenar base stacking.

Table 4. Typical NOE interactions observed in helical A-form conformations.[a]

NOE interaction	Sequential	Intraresidual
H1′ – H8/H6	w	w
H2′ – H8/H6	s	w
H3′ – H8/H6	m	m
H2′ – H1′	w	s
H6/H5	w	s

[a] w = weak (4 – 6 Å), m = medium (2.5 – 4 Å), s = strong (1.5 – 2.5 Å).

By using long mixing times (> 300 ms), spin-diffusion-mediated NOE contacts to the sugar protons H4′, H5′, and H5″ can be observed. However, in most RNA sequences, their assignment is difficult because of the low chemical-shift dispersion in this region. The aromatic – aromatic interresidual NOE contacts in NOESY experiments with long mixing times are very helpful for sequential assignment. In summary, for the NOE-based sequential assignment procedure, a careful analysis of the cross-peaks observed in different experiments yields the desired information.

The pyrimidine H5 and H6 resonances are easy to identify because of the strong NOE cross-signals observed in NOESY experiments with short mixing times. In addition, the signals are split by 7 Hz due to the homonuclear ^3J(H5,H6) coupling. In ^{13}C-labeled RNA, the identical chemical-shift resonances of C6 and C8 can be distinguished by the ^1J(C5,C6) coupling constant of the C6 resonances. Cytosine and uracil can be distinguished by the difference between the chemical shifts of the C5 resonances in both nucleotides.

The assignment of resonances in single-stranded RNA is very difficult; base stacking is missing which leads to a much reduced chemical-shift dispersion. By using NOESY experiments with different mixing times, it is possible to assign the aromatic resonances (H2, H5, H6, and H8) and the sugar resonances (H1′ – H3′). Only in exceptional cases is the assignment of the rest of the sugar protons possible. A sequential assignment breaks at nonpaired nucleotides, for example, bulges. For these regions, isotope labeling of RNA molecules has proven indispensable.

In addition, in ^{13}C- and ^{15}N-labeled RNA, heteronuclear-edited 3D NOESY-HSQC experiments, in which the chemical shifts of the heteronuclei ^{13}C or ^{15}N or both are evolved, can be used for assignment. Some useful experiments are:

- 2D (^{1}H,^{1}H)-NOESY in H_2O with different mixing times
- 2D (^{1}H,^{1}H)-CPMG-NOESY in H_2O[75]
- 3D (^{1}H,^{1}H,^{15}N)-NOESY-HSQC in H_2O
- 3D (^{1}H,^{1}H,^{13}C)-NOESY-HSQC in D_2O
- 3D (^{1}H,^{1}H,^{13}C)-NOESY-HSQC selective for C2, C6, and C8 in H_2O/D_2O
- 3D (^{1}H,^{1}H,^{13}C)-NOESY-HSQC selective for C_{ribose} in D_2O
- For base-specifically labeled RNA molecules or RNA complexes, ω_1-^{13}C-filtered, ω_3-^{13}C-edited 3D (^{1}H,^{1}H,^{13}C)-NOESY-HSQC in D_2O[76]

6.3 Direct correlation of resonances from the nucleobases with resonance from the ribose sugar moiety

Correlation of the nucleobase protons with sugar protons is obtained in HCN triple-resonance experiments in ^{13}C,^{15}N-labeled RNA.[77–82] This experiment is very important for the assignment because of the quite different nitrogen chemical shifts of purines and pyrimidines. In addition, a smaller difference in the ^{15}N chemical shift allows cytosine and uracil to be distinguished (Figure 18).

The easiest implementation of the HCN experiment uses INEPT steps in an out-and-back experiment.[77] The delay for the CH transfer is a compromise for the varying ^1J(C,H) coupling constants: ^1J(C1′,H1′) = 168 Hz, ^1J(C6,H6) = 185 Hz, and ^1J(C8,H8) = 216 Hz. The ^1J(C1′,C2′) coupling constant can be suppressed in the simultaneous t_1 time and CN transfer by either using a constant time delay (CT = 1/^1J(C1′,C2′)),[77] a C2′-selective refocusing pulse,[78]or a C1′-selective inversion pulse.[80] The coherence transfer from the aromatic proton to the nitrogen atom is optimized by using a ^{15}N-selective pulse (150 ppm) to suppress the magnetization transfer to N7 (220 ppm) for purine. The C6/C8 → N1/N9 transfer is optimal for a delay of 40 ms. The transfer efficiency in the HCN experiment was simulated by Wijmenga et al.[2] The simulation reveals that implementation of selective C2′ decoupling provides the best sensitivity. However, a more important role is played by the decoupling of the aromatic carbon atoms C2, C4, and C5 with a C6/C8-selective pulse.

As originally demonstrated for proteins by Grzesiek and Bax,[83] a sensitivity enhancement for larger isotope-labeled proteins or RNA molecules can be obtained in certain cases by evolution of multiquantum (DQ/ZQ coherence, DQ = double quantum, ZQ = zero quantum) instead of single-quantum coherence for HC correlation.[79] For DQ/ZQ coherence, relaxation due to CH dipole – dipole interactions is inactive, which results in a considerable gain in sensitivity. More sensitivity enhancement, at least for correlation peaks involving aromatic carbon atoms, is obtained by exploiting the TROSY effect in the HCN experiment.[81] The combination of TROSY and multiquantum excitation is therefore optimal for larger RNA molecules.[82]

In the HCNCH-type[84] experiments, the HCN experiment is expanded by a relay step. The H1′ proton magnetization is transferred in a manner analogous to the HCN experiment to N1/N9 and forward through C6/C8 to H6/H8. In this experiment, it is necessary to choose an optimal combination of selective pulses, delays, and carrier frequencies for the transfer. For the purine nucleotides, alternative implementations have been reported[85] that use the ^2J(N9,H8) coupling constant (purine: ^2J(N9,H8) = 8 Hz; pyrimidine: ^2J(N9,H8) = 4 Hz) for the direct transfer from N9 to H8.

 © 2003 Wiley-VCH Verlag GmbH & Co. KGaA, Weinheim

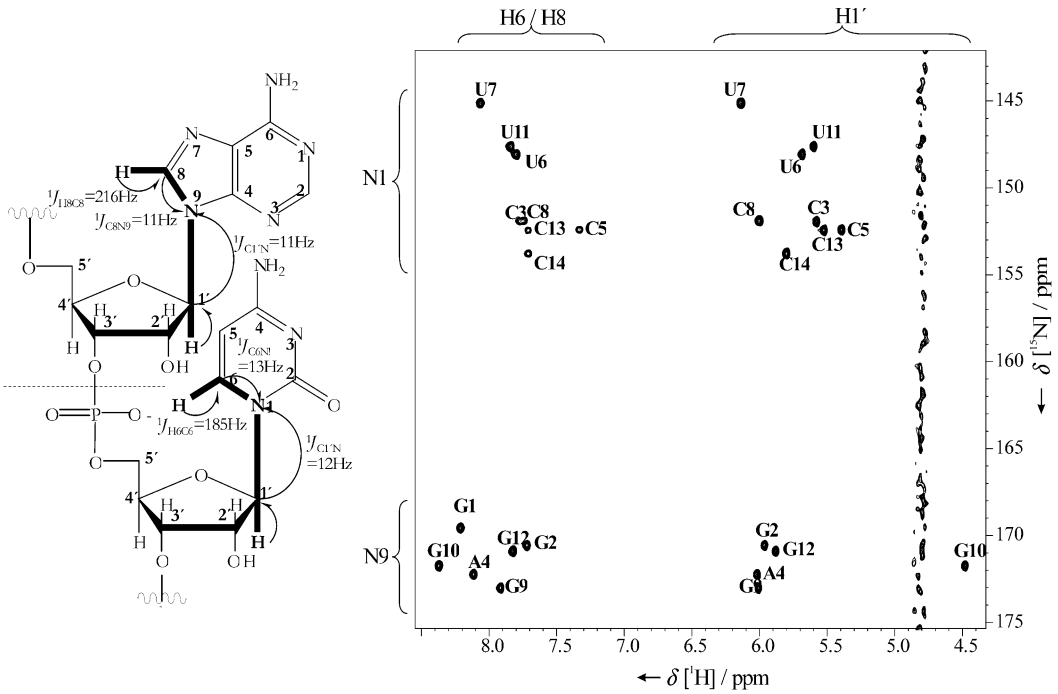

Figure 18. 2D H(C)N experiment at 700 MHz and 298 K for the cUUCGg tetraloop.

6.4 Complete resonance assignment of the nucleobases

As described above, the resonance assignment of the imino and base protons can be derived by using several NOESY experiments with different mixing times. In the next step, the application of standard ^{1}H,^{13}C-HSQC and ^{1}H,^{15}N-HSQC experiments reveal the resonances of the heteroatoms attached to the assigned protons.

For the assignment of the N7 and N9 nitrogen atoms of guanine and adenine and the N1 and N3 atoms of adenine one uses a modified HSQC experiment, the so-called ^{2}J-^{15}N-HSQC.[86] In this experiment, the delay of the INEPT step for magnetization transfer from proton to nitrogen is optimized for the ^{2}J(H,N) coupling. Therefore, this experiment correlates the aromatic protons H8 and H2 with nitrogens N7/N9 and N1/N3, respectively (Figure 19).

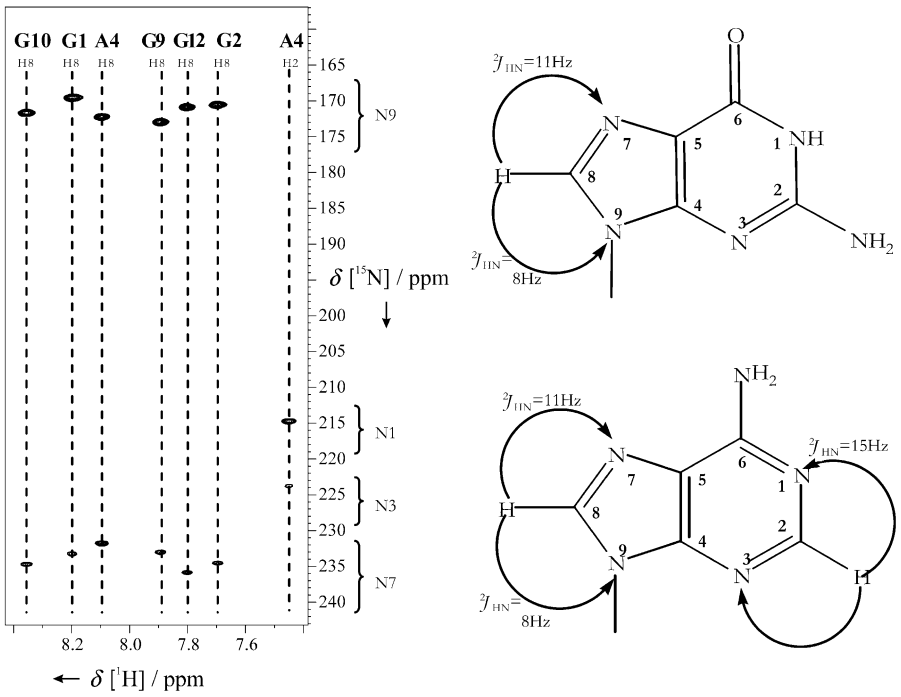

Figure 19. HSQC spectrum at 700 MHz and 298 K with a depiction of the magnetization transfer in adenine und guanine.

With the application of another standard pulse sequence, the 2D HNCO,[87] a correlation between the imino atoms and the C2 and C6 carbon atoms in guanine and C2 and C4 atoms in uracil can be achieved. For the magnetization transfer, subsequent INEPT steps exploit the ^{1}J(H,N) scalar coupling between the imino proton and the attached nitrogen atom and also the scalar coupling ^{1}J(N,C) between the nitrogen atom and the attached carbon atom of the carbonyl group (Figure 20). For the correlation of amino protons in cytosine, which are assignable by using an ^{15}N-HSQC-NOESY experiment, with the carbon atom C4, one applies the same HNCO experiment, the only difference

 © 2003 Wiley-VCH Verlag GmbH & Co. KGaA, Weinheim

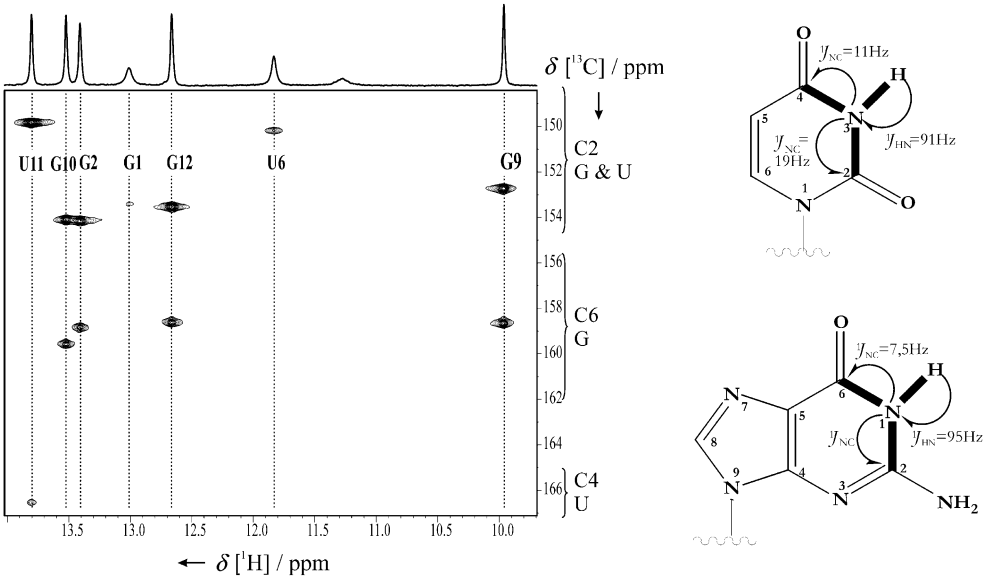

Figure 20. 2D H(N)CO spectrum at 700 MHz and 298 K with a depiction of the magnetization transfer in guanine and uracil.

being that the transmitter frequency of nitrogen is set to the resonance frequency of the amino nitrogen atom at 80 ppm.

For the resonance assignment of the remaining quaternary atoms in the nucleobases two new experiments[6] have been developed. The first one is the so-called HCNC experiment that correlates the aromatic protons and the sugar proton H1′ with the quaternary C4 carbon atom of guanine and C2 of cytosine. The transfer of magnetization is obtained by INEPT steps, which exploit the scalar couplings shown in Figure 21. The advantage of this experiment is that in both cases it starts at protons (either the sugar protons H1′ or the aromatic protons H6/H8) that are well resolved and easy to assign.

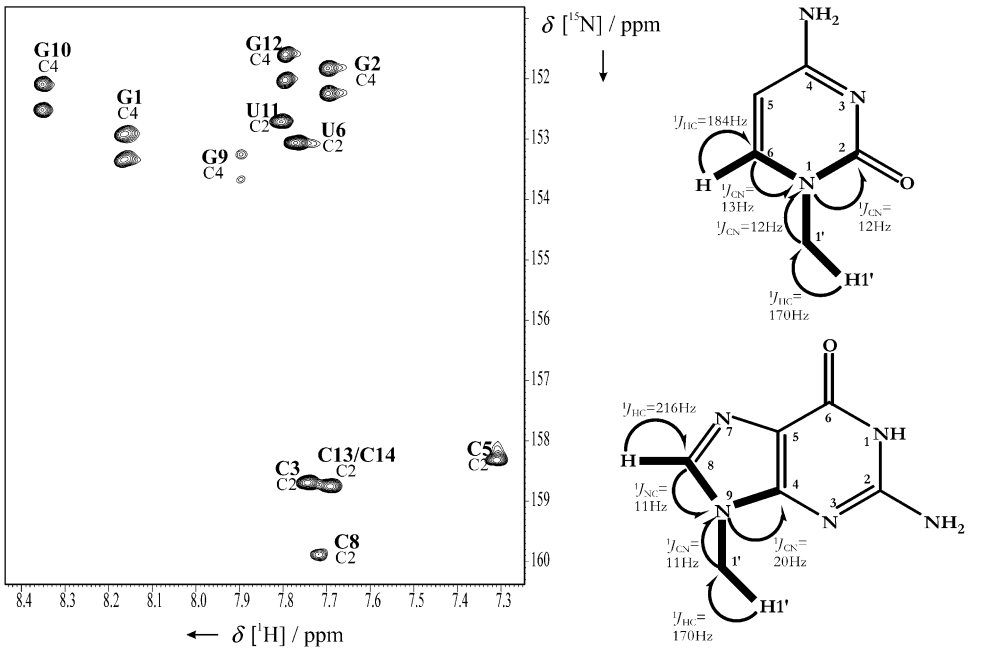

Figure 21. H6/H8 – C6/C8 – N1/9 – C2/C4 experiment at 700 MHz and 298 K with a depiction of the magnetization transfer during the HCNC experiments.

By using a modified HNCOCA experiment,[87] it is possible to assign the quaternary C5 carbon atom in guanine. The resulting pulse sequence is called HNC6C5, named after the pathway of magnetization. The experiment uses selective INEPT steps to correlate the imino proton with the quaternary carbon atom C5. As depicted in the spectrum (Figure 22), the dispersion of chemical shifts for these atoms is limited, but it is sufficient to obtain a complete resonance assignment of all NMR-active nuclei in the nucleobases.

6.5 Complete assignments of sugar atoms

Based on the sequential assignment of the H1′ protons, one needs just a single experiment, the 3D forward-directed HCC-TOCSY-CCH-E.COSY,[88–90] to assign all the remaining atoms in the sugar moieties of the RNA molecule. In this experiment, the ^{1}H and ^{13}C atoms of the ribose ring are correlated by two sequential transfer steps, a CC-TOCSY and a COSY, by exploiting the large scalar ^1J(C,H) and ^1J(C,C) couplings that depend only to a small degree on the conformation of the nucleotide. This experiment is also advantageous in comparison to the normal HCCH-TOCSY experiments[91] because the resolution is much higher. In this optimized 3D experiment, one observes the peaks of the type Ci′H$i+1$′ (with $i = 1-4$, sugar nomenclature) of every single nucleotide in a frequency plane that is edited with the chemical shift of the well-resolved corresponding H1′ proton. The resonance assignment is obtained by choosing the distinct ^{1}H,^{13}C frequency planes edited with the corresponding H1′ proton chemical shift in the ^{1}H – ^{1}H projection. By comparing these planes to the ^{1}H,^{13}C-HSQC spectrum, all signals of one spin system, according to a ribose moiety, can be correlated and assigned (Figure 23).

Sequential assignment of adjacent sugar moieties can be obtained by using the 3D HCP experiment.[92–94] In this experiment, H3′$_i$C3′$_i$ and H4′$_i$C4′$_i$ resonances are correlated with P$_{i+1}$ on the 3′ side and the H5′$_i$/H5″$_i$C5′$_i$ and H4′$_i$C4′$_i$ resonances are correlated with P$_i$ on the 5′ side of the phosphodiester backbone. This allows not only a sequential assign-

 © 2003 Wiley-VCH Verlag GmbH & Co. KGaA, Weinheim

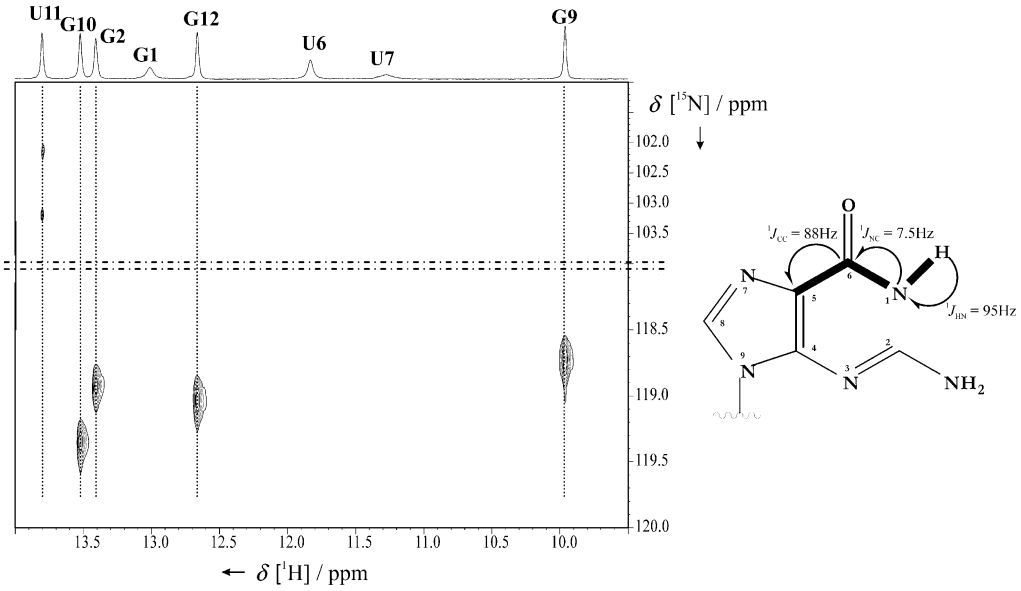

Figure 22. 2D H(NC)C spectrum at 700 MHz and 298 K with schematic presentation of the magnetization transfer in guanine.

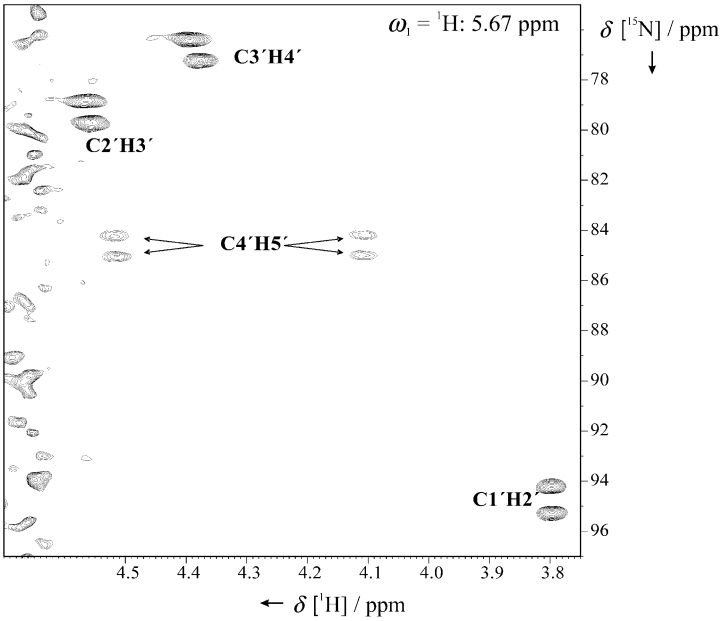

Figure 23. $^1H,^{13}C$ plane at $\omega_1 = \{^1H\} = 5.674$ ppm in forward-directed HCC-TOCSY-CCH-COSY experiments at 600 MHz and 298 K for the UUCG tetraloop.

ment of the C4′H4′ resonances but also a partial assignment of the resonances in the ribose spin system. The magnetization transfer is similar to those in the CT-HNCO and HCN experiments and follows an out-and-back manner with sequential INEPT steps (Figure 24).

For small RNA molecules, the 3D HCP experiment can be extended by an additional CC-TOCSY transfer step to directly correlate the phosphorous resonances with the well-resolved C1′H1′ region of the spectrum.[95]

7. Conformation Analysis with Chemical Shifts

The chemical shift is a sensitive measure for RNA conformation. Unusual conformations can be detected by comparing the referenced chemical shifts of the examined RNA with the data deposited in the BMRB database. Such a procedure can be applied to all NMR-active nuclei. The dependence of ^1H chemical shifts on secondary structure has been analyzed in detail for a number of different RNA molecules including the cUUCGg tetraloop[96] and shall not be discussed here.

^{31}P chemical shifts and their deviations from standard chemical shifts in A-form RNA are often taken to be indicative for unusual conformations around the phosphodiester backbone. It is possible to calculate the deviations in the ^{31}P chemical shift from the mean value of the assigned RNA molecules deposited in the BMRB database. In the cUUCGg tetraloop, significant variations for the phosphorous chemical shift are observed for the loop residues U7, C8, G9, and the nucleotide G10 that is part of the closing base pair (Figure 25 C). The chemical shifts of the residues in canonical A-form conformation are not significantly different from the mean value.

^{13}C chemical-shift data yielding the sugar pucker modes could be obtained following the sophisticated analysis of solid-state NMR data by Ebrahimi et al.[97] For this analysis, canonical coordinates were calculated by using the chemical-shift data (δ) according to Equations 1 and 2.

$$can1 = 0.179\delta_{C1'} - 0.225\delta_{C4'} - 0.0585\delta_{C5'} \quad (1)$$

$$can2 = -0.0605(\delta_{C2'} + \delta_{C3'}) - 0.0556\delta_{C4'} - 0.0524\delta_{C5'} \quad (2)$$

The first canonical coordinate *can*1 describes the pseudorotation phase of the sugar moiety. For *can*1 > -6.25 ppm, the

 © 2003 Wiley-VCH Verlag GmbH & Co. KGaA, Weinheim

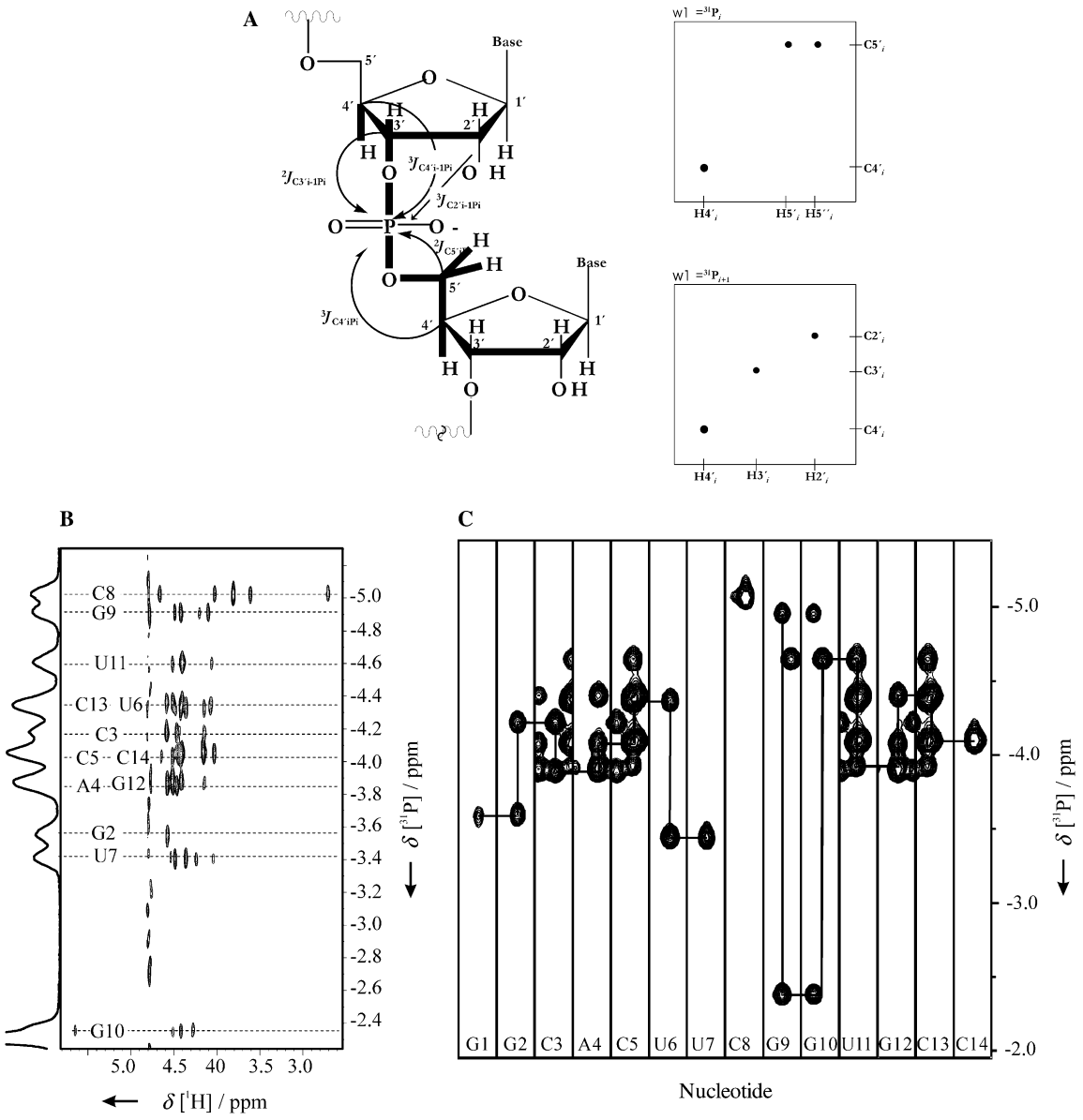

Figure 24. A) Representation of the HCP experiment on the left. The correlated atoms in the experiment are indicated through the exploited scalar coupling represented by arrows. The right-hand side shows the expected 2D ^{1}H-^{13}C plane of the 3D experiment at different phosphorous chemical shifts. The C4′H4′ resonance of one ribose unit is correlated with two phosphorous resonances, P_i and P_{i+1}. The C2′H2′ and the C3′H3′ are correlated with P_{i+1} and C5′H5′/H5′′ with P_i; the C4′H4′ unit shows cross-peaks to both P_i and P_{i+1}. B) ^{1}H, ^{31}P projection of the 3D HCP spectrum of the cUUCGg tetraloop. C) The 3D HCP experiment in form of a strip plot. The sequential assignment pathway is indicated.

sugar is in a C3′-endo conformation, for *can*1 < -6.25 ppm, the sugar adopts a C2′-endo conformation. The second coordinate *can*2 determines the conformation of the exocyclic torsion angle γ. If the torsion angle γ is in a gauche–gauche conformation ($\gamma = +60°$), *can*2 $\geqslant -16.8$ ppm. Population of either of the two gauche–trans conformations ($\gamma = -60°$, 180°) results in a coordinate *can*2 smaller than -16.8 ppm. Application of these rules to the chemical-shift data of the cUUCGg tetraloop allows clear discrimination between residues with different sugar pucker modes (Figure 25 A). According to this analysis, residues C8 and U7 adopt a C2′-endo conformation; while all other residues are in C3′-endo conformation. The coordinate analysis fails for residue G1, maybe due to a higher conformational flexibility at the 5′ end of the stem or due to the additional charge that alters the chemical shifts. These results are in good agreement with the published structures and are also in very good agreement with the analysis of scalar ^{3}J(H,H) coupling constants and cross-correlated relaxation rates in the ribose ring.

Discrimination between gg and gt conformations and the exocyclic torsion angle γ on the basis of *can*2 is less convincing. Most of the values of *can*2 are clustered in the region between -16.6 and -17.0 ppm. Only the nucleotides G1, U7, C8, G9, and G10 are clearly in the gg conformation. The uncertainty in the analysis could be due to the simultaneous use of the chemical shifts of C2′ and C3′ in the calculation. For the tetraloop, the

 © 2003 Wiley-VCH Verlag GmbH & Co. KGaA, Weinheim

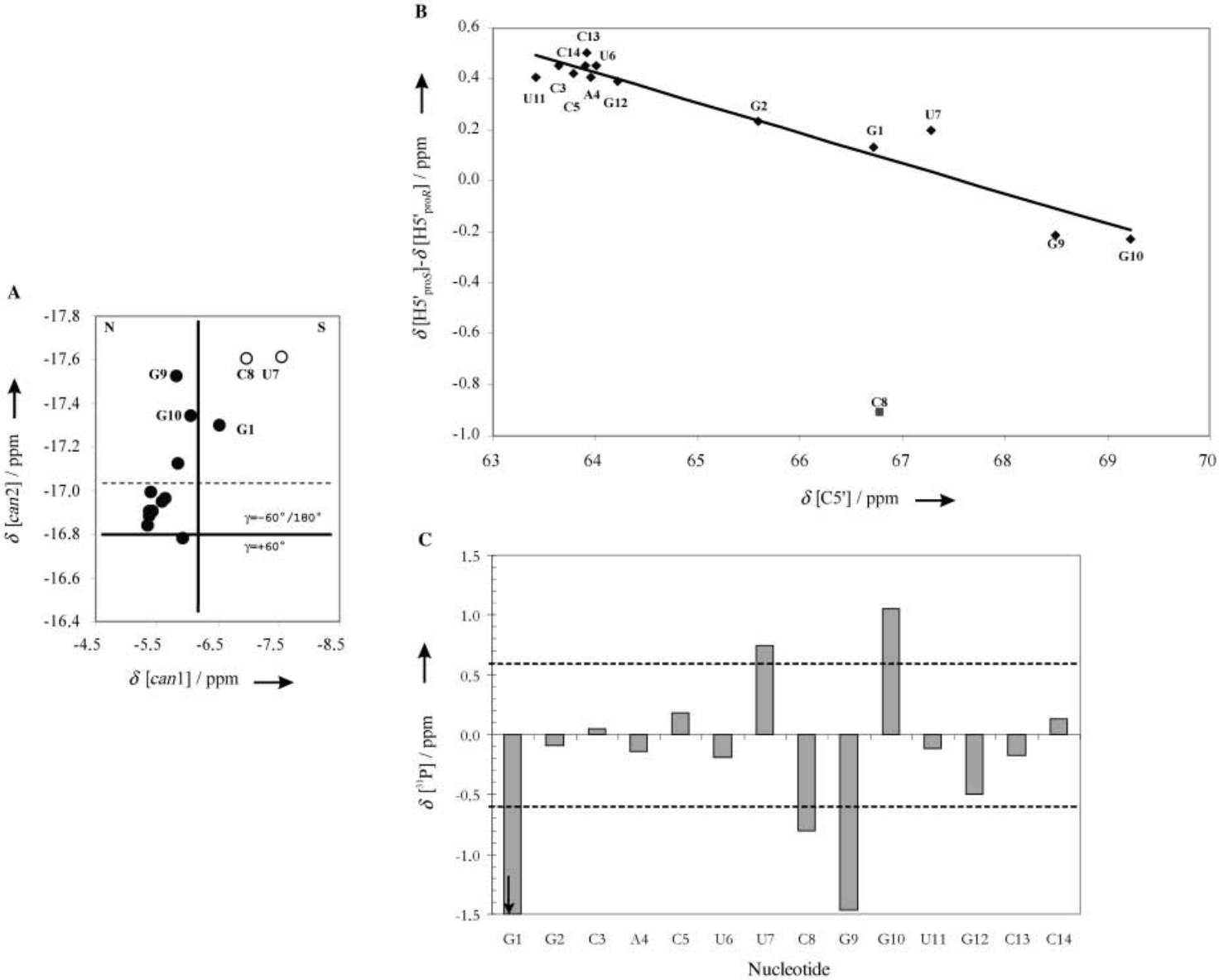

Figure 25. Chemical-shift analysis for the determination of: A) the sugar pucker mode and the exocyclic torsion angle γ (from the work of Ebrahimi et al.[97]), B) the stereospecific assignment of the H5′ and H5″ protons in RNA (from the work of Marino et al.[89]), and C) the conformation of the phosphodiester backbone (from the work of Fürtig et al.[6]).

analysis would predict residues with *can*2 < -17 ppm to be in a gg conformation around the exocyclic torsion angles γ.

By analyzing the chemical-shift data of the C5′H5′/C5′H5″ resonances, a stereospecific assignment of the prochiral H5′/H5″ protons was obtained. It is observed that in helical RNA structures, the resonance of the H5′(pro-*S*) proton is shifted up-field with regard to the resonance of the H5′(pro-*R*) proton.[98] This rule is unfortunately not applicable to noncanonical regions of RNA structures. However, a stereospecific assignment is possible by correlation of the difference in the proton chemical shifts of the pro-*S* and pro-*R* protons with the respective carbon chemical shift, $\Delta\delta$[H5(pro-*S*) − H5(pro-*R*)](δ^{13}C).[89] If one depicts the differences of the proton chemical shifts versus the carbon chemical shift, the stereochemical assignment is revealed (Figure 25 B). A general *anti* correlation could be observed for the carbon chemical shift of these resonances. An exception is residue C8; this is probably the result of the different conformation of γ at this loop position. These results are in good agreement with the data obtained from the analysis of the ^2J(C4′,H5′/H5″) and ^3J(H4′,H5′/H5″) coupling constants.

8. Delineation of Secondary Structure Motifs such as Hairpins and Bulges

Many RNA structures are built up in a modular fashion from smaller structural elements that fold autonomously and are stable on their own. Due to their noncanonical structure, some of these structural elements give rise to resonances in the NMR

 © 2003 Wiley-VCH Verlag GmbH & Co. KGaA, Weinheim

spectra with unusual chemical shifts outside of the standard chemical-shift ranges. Furthermore these chemical shifts are often similar when such a modular element is present in different contexts in different RNA molecules. A classical example of this is the UNCG family of stable tetraloops. The tight fold of the loop with an unusual U:G base pair, a guanine residue in the *syn* conformation, and a cross-strand stacking interaction between the first and the third loop-nucleotides[8] results in a number of NMR signals far outside the usual chemical-shift ranges[59] (Figure 26 A). These chemical-shift patterns do not change when the loop is inserted into other RNA molecules (Figure 26 B) and due to their good separation from the bulk of the other signals they can still be recognized and the presence of a UNCG loop element can be verified. A similar fingerprint of unusually shifted resonances can be found for another family of stable tetraloops, the GNRA tetraloops.[99–101] A further example of a structural motif giving rise to a specific chemical-shift pattern might be provided by the loop E-motif. The loop E-motif[102] occurs in a variety of internal bulges in different RNA molecules such as 5S rRNA,[103, 104] the ribosomal sarcin loop,[100, 101] the hairpin ribozyme domain B,[105] and viroids.[106] However, with the availability of more completely assigned and structurally characterized RNA molecules, the connection between chemical-shift patterns and conserved structural elements will become clearer and more motifs might be found.

9. Determination of Local Conformation and Conformational Dynamics in RNA

The conformation of the phosphodiester backbone and the ribosyl furanoside plays a dominant role in preorganizing the overall structure of a nucleic acid. Therefore, the properties and interaction possibilities of an RNA molecule depend on the conformation and the dynamics of the ribose ring and the phosphodiester backbone.

The determination of the pseudorotation phase P and pseudorotation amplitude ν_{max} of the ribose moiety is based on the interpretation of homonuclear ^3J(H,H) coupling constants. The sugar pucker in canonical A-form RNA is C3′-endo. In this conformation, the orientation of H1′ to the H2′ proton is synclinal and one observes a small ^3J(H1′,H2′) coupling constant. The H3′ and H4′ protons are in an antiperiplanar orientation and one observes a large ^3J(H3′,H4′) coupling constant. In contrast, small ^3J(H3′,H4′) and large ^3J(H1′H2′) coupling constants are the signature for a ribose sugar moiety in C2′-endo conformation. The ^3J(H2′,H3′) coupling constant cannot be used for differentiation because in both conformations its value is around 4 Hz. The dependence of the ^3J(H,H) coupling constants on the sugar conformation is shown in Figure 27.

The homonuclear ^3J(H,H) coupling constants for two RNA hairpins (the cUUUUg loop and cUUCGg loop) have been determined in the forward-directed HCC-TOCSY-CCH-E.COSY experiment (Figure 28),[88, 90] and Table 5 provides a summary of the extracted coupling constants. The pseudorotation phase P and amplitude ν_{max} can be calculated by using the parameterization of Haasnoot et al.[107–109] The results (see Table 5) for the cUUUUg loop show that U4 is in a C3′-endo conformation whereas the ribose rings of U5 and U7 adopt C2′-endo conformations. The coupling constants of U6 cannot be explained with one static conformation of the ribose ring. Therefore, the sugar moiety of this nucleotide must be flexible and can be modeled under the as-

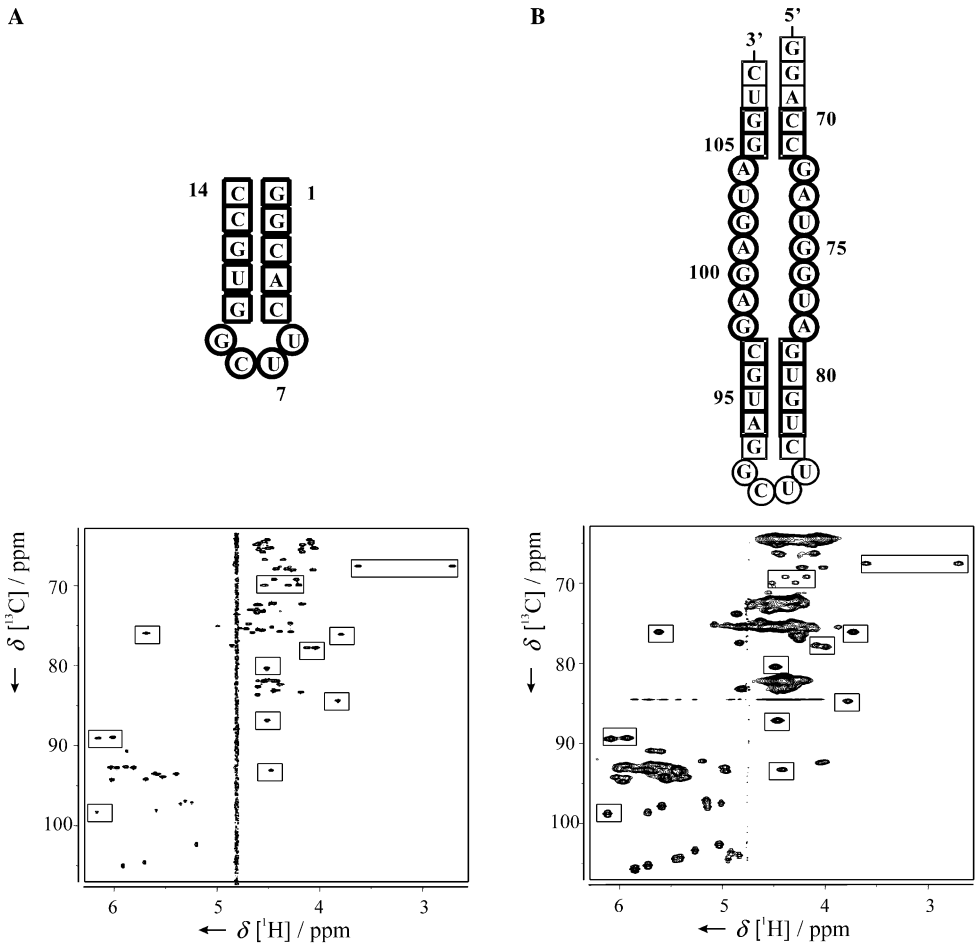

Figure 26. Identification of a UUCG stable tetraloop motif in two different RNA molecules by the chemical-shift signature. A) ^{1}H,^{13}C-HSQC spectrum of a small hairpin RNA closed by a stable tetraloop with resonances exhibiting unusual chemical shifts due to the tetraloop fold indicated in boxes. B) ^{1}H,^{13}C-HSQC spectrum of a larger RNA containing a similar tetraloop. Again the resonances belonging to the loop are marked in boxes.

 © 2003 Wiley-VCH Verlag GmbH & Co. KGaA, Weinheim

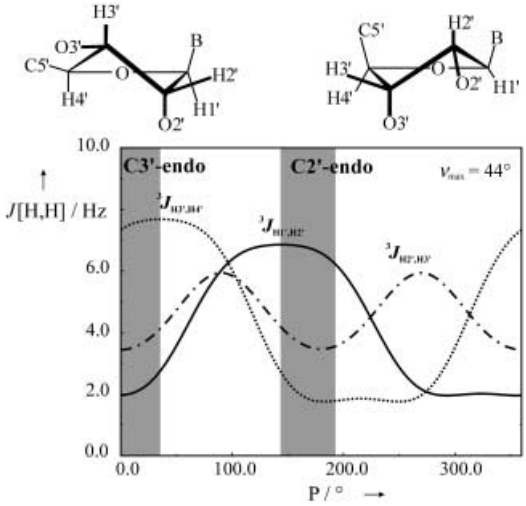

Figure 27. Karplus relation of ^3J(H1′,H2′), ^3J(H2′,H3′), and ^3J(H3′,H4′) coupling constants depending on the pseudorotation phase P at a pseudorotation amplitude ν_{max} of 44°.

sumption of an equilibrium between the C2′- (37%) and C3′-endo (63%) conformations. This result is consistent with those obtained when measuring a larger set of heteronuclear ^nJ(C,H) coupling constants[110] or cross-correlated relaxation rates.[111]

While the cUUUUg loop shows conformational flexibility in at least one of the ribose moieties of the loop nucleotides, the cUUCGg-loop nucleotides adopt more rigid sugar conformations. The ribose rings of U6 and G9 adopt canonical A-form conformations whereas the ribose rings of U7 and C8 adopt B-form conformations. The scalar coupling data (Figure 29) indicate that in the case of the cUUCGg loop, the closing base G10 might adopt an unusual sugar conformation. If one interprets the values of the coupling constants as mean values of two differently populated canonical conformations, the values must be based on an equilibrium between 67% in A- and 33% in B-form conformations for nucleotide G10.

Measurement of ^3J(H,H) coupling constants provides a valuable tool for describing the conformation, including the dynamic equilibria, of the sugar rings that determines the overall conformation. A further discussion of available NMR parameters for the determination of the phosphodiester backbone has been provided previously (by Schwalbe et al.[112] and by Griesinger et al.[113]). Table 6 summarizes the NMR parameters available for the determination of dihedral angles in RNA: homo- and heteronuclear vicinal coupling constants (^3J) and cross-correlated relaxation rates (Γ rates).

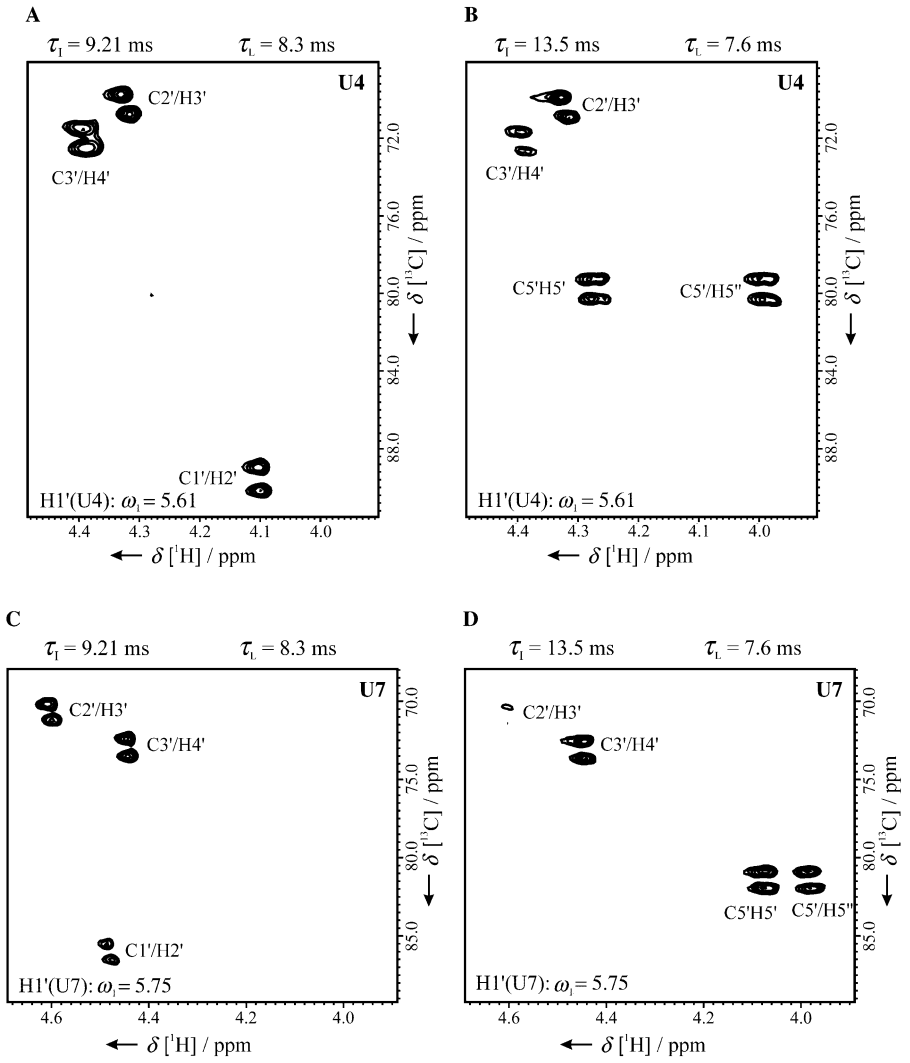

Figure 28. Forward-directed HCC-TOCSY-E.COSY spectra for 1.5 mM UUUU tetraloop RNA. A, C) Correlation from C1′ – C3′. B, D) Correlation from C4′ – C5′.

10. RNA Global Structure: Residual Dipolar Couplings

A notorious problem in the structure determination of RNA based on NOE contacts and scalar couplings is the absence of long-range NOE contacts due to the often elongated rodlike helical structures of RNA. The short-range nature of the NOE information does not allow a precise definition of the relative spatial orientation of distant parts of the molecule. Therefore, it is difficult to extract information about helical bend and end-to-end orientation or interhelical angles for different helical parts of a molecule. Here residual dipolar couplings (RDCs) present a new source of structural information that can be used to overcome these obstacles. RDCs contain global structural information since they report on the orientation of individual bond vectors with regard to the axes of the alignment tensor of the molecule. They

 © 2003 Wiley-VCH Verlag GmbH & Co. KGaA, Weinheim

Table 5. *Experimental homonuclear proton coupling constants for the cUUUUg and cUUCGg tetraloops extracted from forward-directed HCC-TOCSY-CCH-E.COSY spectra.*

	cUUUUg loop				cUUCGg loop			
	U4	U5	U6	U7	U6	U7	C8	G9
^3J(H1′,H2′)[a]	2.6 ± 0.3	8.7 ± 0.1	6.8 ± 0.1	8.1	0.2	8.0	9.3	0.6
^3J(H2′,H3′)[a]	5.2 ± 0.3	5.5 ± 0.1	5.4 ± 0.1	5.4 ± 0.3	5.5	5.2	4.9	3.4
^3J(H3′,H4′)[a]	8.9 ± 0.2	1.6 ± 0.2	4.7 ± 0.1	3.1 ± 0.2	11.0	1.0	0.6	7.6
rms$J$[b]	0.42	0.42	1.07	0.24	1.3	0.2	0.7	0.6
Pseudorotation amplitude[c] (ν_{max})	44	43	42	44	43	38	44	44
Pseudorotation phase[c] (P)	44	144	123	134	29	160	155	16

[a] Average coupling values; determination of the coupling constant at two different submultiplets. [b] rms$J = (\Sigma(J_{theo} - J_{exp})^2)^{-1/2}/(n)^{-1/2}$ measured in Hz, where n is the number of couplings. [c] Prediction with the parameters described in the work of Haasnoot et al.[107–109]

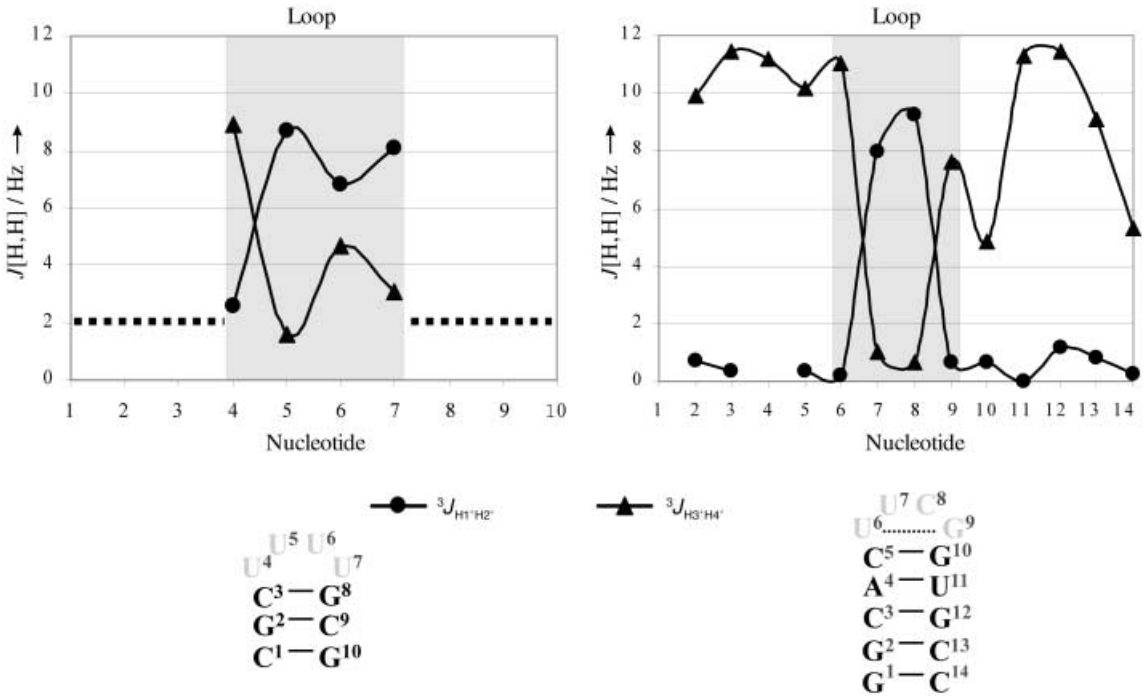

Figure 29. *Depiction of the scalar couplings ^3J(H1′H2′) and ^3J(H3′H4′) versus the nucleotide sequence. In the lower part of the figure, the corresponding secondary structures of the molecules are depicted. Grey numbers of the nucleotide indicate that these nucleotides are ^{13}C- and ^{15}N-labeled. Loop nucleotides are depicted in grey like the loop region of the plots.*

Table 6. *Experimental parameters available for the determination of the local conformation (α, β, γ, δ, ε, ζ, χ, P, and ν_{max}) of RNA molecules.*

Structural parameter	NMR spectroscopy parameter			Ref.
	Cross-correlated relaxation rates	Homonuclear ^3J coupling constants	Heteronuclear ^3J coupling constants	
backbone:				
α	$\Gamma^{DD,CSA}_{C'_iH'_i,P'_i}$			[141]
β	$\Gamma^{DD,DD}_{H5'_iC5'_i,H5''_iP'_i}$		^3J(H5′,P), ^3J(H5″,P), ^3J(C4′,P)	[142 – 147]
γ		^3J(H4′,H5′), ^3J(H4′,H5″)	^3J(C3′,H5′), ^3J(C3′,H5″)	[88, 89, 110, 148]
δ		^3J(H3′,H4′)	^3J(C5′, H3′), ^3J(C2′,H4′)	[88, 89, 110]
ε	$\Gamma^{DD,DD}_{H3'_iC3'_i,H3'_iP'_{i+1}}$		^3J(H3′,P), ^3J(C2′,P), ^3J(C4′,P)	[142 – 147, 149, 150]
ζ	$\Gamma^{DD,CSA}_{C3'_iH3'_i,P_{i+1}}$			[141]
glycosidic bond: χ	$\Gamma^{DD,CSA}_{C1'H1',N}$, $\Gamma^{DD,CSA}_{C2'H2',N}$		^3J(C6/C8,H1′), ^3J(C4/C2,H1′)	[143, 151, 152]
ribose moiety: ν_{max}, P	$\Gamma^{DD,DD}_{C1'H1',C2'H2'}$, $\Gamma^{DD,DD}_{C3'H3',C4'H4'}$	^3J(H1′,H2′), ^3J(H3′,H4′)	^3J(C,H)	[88, 110, 111, 153]
hydrogen bonding	$\Gamma^{DD,DD}_{NH,N...H}$, $\Gamma^{CSA,CSA}_{N,N}$, $\Gamma^{DD,CSA}_{NH,H}$		^{h3}J(N,N), ^{h2}J(H^N,N)	[32, 154, 155]

are caused by the presence of an aligning medium that interferes with the isotropic tumbling of a molecule and induces a certain degree of alignment of the molecule with respect to the magnetic field. Alignment media that have been used for nucleic acids are filamentous phages[114] introduced by Pardi and co-workers, *n*-alkyl-polyethylene glycol/*n*-alkyl-alcohol bi-

 © 2003 Wiley-VCH Verlag GmbH & Co. KGaA, Weinheim

celles,[115, 116] and the magnetic field itself.[117, 118] The introduction of orientation restraints derived from residual dipolar couplings leads to a higher precision of the derived structures in standard structure determinations (for examples, see refs. [119–122]), especially in loop regions where NOE contacts tend to be more scarce.[116] A further improvement of structure determinations can be expected from the measurement of more exotic dipolar couplings such as PH couplings between protons in the bases and the phosphorus nuclei in the RNA backbone,[123] since they report on the conformation of the backbone, which is notoriously underdefined in classical NMR structure determinations due to the low proton density along the backbone. In addition,

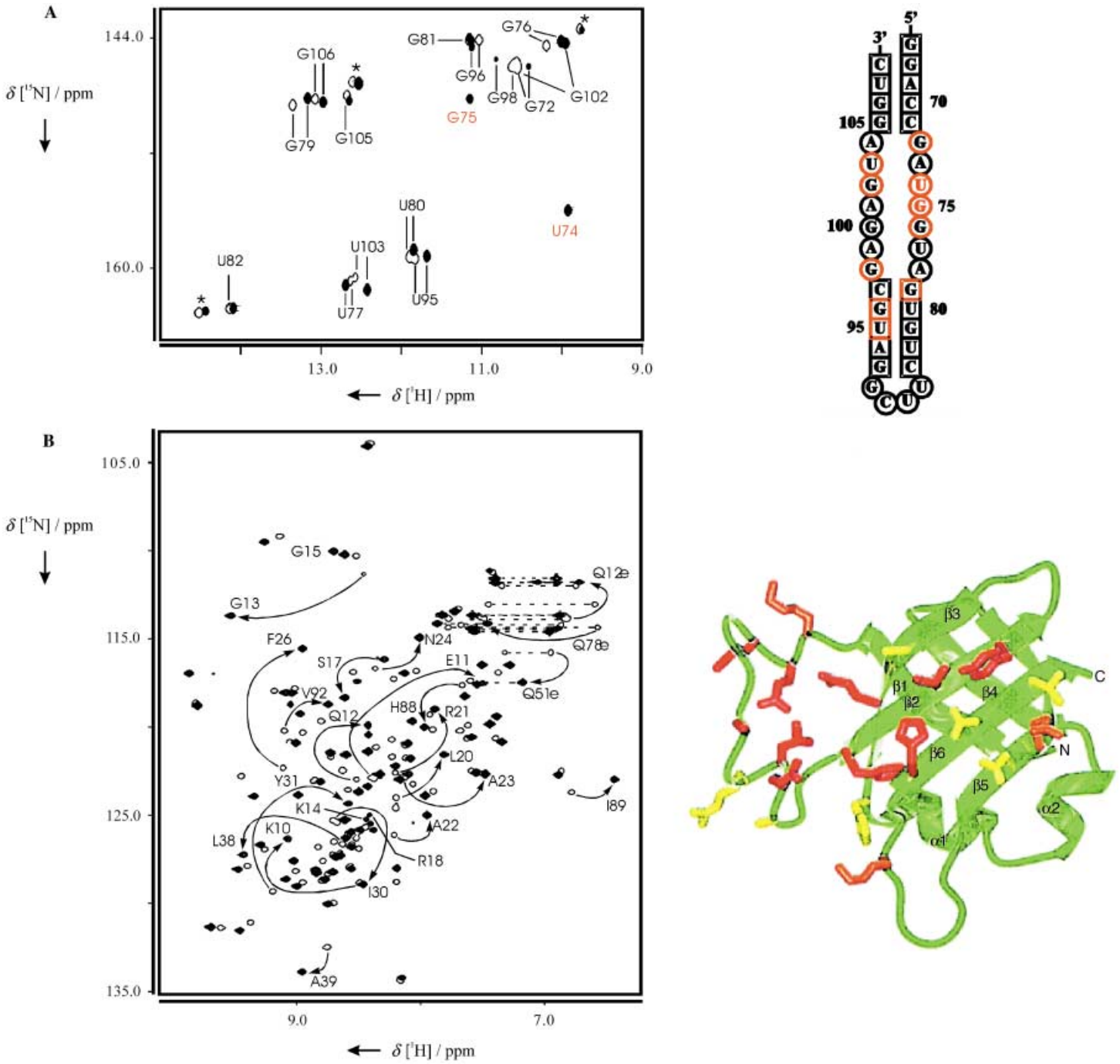

Figure 30. Identification of the interaction surfaces in the complex of the E. coli 5S rRNA E-loop and ribosomal protein L25 by chemical-shift mapping (from the work of Stoldt et al.[132]). A) Left: $^{1}H,^{15}N$-HSQC spectrum of 5SE RNA in the absence (open contours) and the presence (filled contours) of rL25 with the assignments indicated. Residues labeled in red are only observable in the bound state due to protection from fast exchange with the solvent in the presence of the protein. Right: Mapping of residues with substantial chemical-shift changes (red circles) or protection from solvent exchange (red squares) onto the secondary structure of 5SE RNA to reveal a bipartite protein binding site. B) Left: $^{1}H,^{15}N$-HSQC spectrum of rL25 in the absence (open contours) and the presence (filled contours) of 5SE RNA with the assignments indicated. Right: Mapping of residues with substantial chemical-shift changes onto the structure of rL25 in the RNA-free form (from the work of Stoldt et al.[132]).

 © 2003 Wiley-VCH Verlag GmbH & Co. KGaA, Weinheim

^{1}H,^{1}H residual dipolar couplings[124] can potentially be used as sources for long-range distances and for orientation information.

However, the full potential of RDCs as constraints is shown when in the definition of global structural features such as interhelical angles, for example, in the complex of the U1A protein with its target RNA,[125] the theophylline aptamer complex,[126] or the domain orientation in tRNA molecules.[127] The example of tRNA already shows that it is possible to derive structural information for larger RNA molecules that are normally not amenable to a full structural characterization by NMR spectroscopy. In a study of the hammerhead ribozyme[128] it was shown that the relative orientations of the three helical parts in the absence of magnesium in solution is totally different to the crystal structure and major interhelical reorientations have to occur before the ribozyme folds into its catalytically active conformation. Furthermore, it is possible to align ligands and their target RNA with respect to each other without the need for a full structure determination, based on RDC information.[129] In addition, Patel's group used residual dipolar couplings to obtain information on RNA dynamics in the case of HIV1-Tar RNA with respect to interhelical motions;[130] this indicated that the free RNA was already able to sample conformations of the ligand-bound state. RDCs also appear to have the potential to speed up RNA structure determination in general in structural genomics approaches.[131]

11. Mapping of Interaction Surfaces of RNA Molecules

Many RNA molecules carry out their function in complex with ligands, such as proteins, other RNA molecules, or small molecules or metal ions. It is often of interest to determine the functional groups of an RNA molecule that interact with these ligands for guiding mutational studies, for interpreting phylogenetic data such as sequence conservation, or for other biological questions. Sometimes the biophysical properties of RNA – ligand complexes are detrimental to solving a complete structure of the complex or even assigning the RNA in its bound state due to, for example, a large size, a limited solubility, or unfavorable kinetic behavior of the complex. However, even in such cases it is possible to obtain information on RNA groups involved in binding. The most straightforward method is the observation of chemical-shift changes of the RNA upon gradual addition of the ligand—a method called chemical-shift mapping. Probably the first application of this method to RNA was reported by Kime and Moore in 1983[31] in an investigation of the binding of the ribosomal protein L25 to 5S rRNA from *E. coli*. In their pioneering work, they used changes in the 1D ^{1}H spectra of the imino proton region of 5S rRNA upon addition of rL25 to identify nucleotides in the E-loop region of 5S rRNA as the possible protein binding site. It then took sixteen more years to characterize the binding of rL25 to the 5S rRNA E-loop in atomic detail, both by NMR spectroscopy[132] and X-ray crystallography.[133] The example of the $\approx$120 nucleotide 5S rRNA indicates that chemical-shift mapping can be used even for larger RNA molecules that are beyond a complete structural characterization with current NMR methods. Ligand binding often does not only induce chemical-shift changes but allows the observation of imino proton resonances that are not observable or are broadened in the free RNA due to fast exchange with the solvent (Figure 30); this occurs either by stabilization of the RNA structure (for example, see ref. [134]) or by protection of the imino protons from exchange (for example, see refs. [135, 136]) by direct RNA – protein contacts. Chemical-shift mapping is also applicable in cases when RNA – protein complexes of lower affinity are formed and the components are in fast or intermediate exchange on the NMR timescale (for example, see ref. [137]).

An alternative to the chemical-shift mapping approach is to use cross-saturation experiments.[138] In these experiments, resonances of one component of a biomolecular complex are selectively saturated. By spin diffusion, this saturation is transferred to the second component of the complex, thereby leading to a loss of the signal intensities of its NMR spectra resonances. The largest effects are observed for residues close to the interface of the complex, which allows the identification of residues that are part of the interaction surface. In RNA – protein complexes one can take advantage of the fact that there are numerous spectral windows where protein and RNA resonances do not overlap, for example, the region of the RNA imino protons, the RNA H1′ protons, and the region of the aliphatic resonances of the protein upfield of 2 ppm. This makes the selective irradiation of one of the binding partners especially straightforward.[139] In addition, since the detection is mostly done by using highly sensitive HSQC spectroscopy this method appears to be applicable to larger complexes.[140]

Acknowledgements

The authors would like to thank Matthias Görlach, Matthias Stoldt, Christian Sich, Oliver Ohlenschläger, Ramadurai Ramachandran, Christian Griesinger, Elke Duchardt, Wolfgang Bermel, John Marino, Mirko Hennig, Steffen Glaser, and Bernd Reif for many interesting discussions about all aspects of RNA structure, biochemistry, and NMR spectroscopy. We are grateful to Matthias Stoldt, Matthias Görlach, and Elke Duchardt for help with figures and for sharing data prior to publication. We are grateful to Aphrodite Anastasiadis-Pool and Emily S. Collins for reading the manuscript. The work has been supported by the state of Hesse, the European Large-Scale Facility, the Sonderforschungsbereich 579 "RNA – Ligand Interactions", and the Fonds der Chemischen Industrie.

Keywords: conformation analysis · isotope labeling · NMR spectroscopy · resonance assignment · RNA

[1] G. Varani, F. Aboul-ela, F. H.-T. Allain, *Progress in NMR spectroscopy* **1996**, *29*, 51 – 127.
[2] S. S. Wijmenga, B. N. M. van Buuren, *Progress in NMR spectroscopy* **1998**, *32*, 287 – 387.
[3] R. T. Batey, M. Inada, E. Kujawinski, J. D. Puglisi, J. R. Williamson, *Nucleic Acids Res.* **1992**, *20*, 4515 – 4523.
[4] E. P. Nikonowicz, A. Sirr, P. Legault, F. M. Jucker, L. M. Baer, A. Pardi, *Nucleic Acids Res.* **1992**, *20*, 4507 – 4513.
[5] P. Büchner, W. Maurer, H. H. Rüterjans, *J. Magn. Reson.* **1978**, *29*, 45 – 63.

 © 2003 Wiley-VCH Verlag GmbH & Co. KGaA, Weinheim

[6] B. Fürtig, C. Richter, W. Bermel, H. Schwalbe, *J. Biomol. NMR* **2003**, in press.
[7] E. Ennifar, A. Nikulin, S. Tishchenko, A. Serganov, N. Nevskaya, M. Garber, B. Ehresmann, C. Ehresmann, S. Nikonov, P. Dumas, *J. Mol. Biol.* **2000**, *304*, 35 – 42.
[8] F. H.-T. Allain, G. Varani, *J. Mol. Biol.* **1995**, *250*, 333 – 353.
[9] D. J. Proctor, J. E. Schaak, J. M. Bevilacqua, C. J. Falzone, P. C. Bevilacqua, *Biochemistry* **2002**, *41*, 12 062 – 12 075.
[10] C. Kojma, M. A. Ono, A. Ono, M. Kainosho, *Meth. Enzymol.* **2001**, **338**, 261 – 282.
[11] I. M. Lagoja, P. Herdewijn, *Synthesis* **2002**, *3*, 301 – 314.
[12] S. S. P. Quant, R. W. Wechselberger, P. Schell, J. W. Engels, C. Griesinger, H. Schwalbe, *Tetrahedron Lett.* **1994**, *35*, 6649 – 6652.
[13] M. Chamberlin, J. Ring, *J. Biol. Chem.* **1973**, *248*, 2235 – 2250.
[14] E. T. Butler, M. J. Chamberlin, *J. Biol. Chem.* **1982**, *257*, 5772 – 5778.
[15] J. F. Milligan, D. R. Groebe, W. G. Witherell, O. C. Uhlenbeck, *Nucleic Acids Res.* **1987**, *15*, 8783 – 8798.
[16] J. R. Wyatt, M. Chastain, J. D. Puglisi, *Biotechniques* **1991**, *11*, 764 – 769.
[17] W. T. Stump, K. B. Hall, *Nucleic Acids Res.* **1993**, *21*, 5480 – 5484.
[18] J. F. Milligan, O. C. Uhlenbeck, *Meth. Enzymol.* **1989**, *180*, 51 – 62.
[19] C. A. Grosshans, T. R. Cech, *Nucleic Acids Res.* **1991**, *19*, 3875 – 3880.
[20] A. R. Ferre-D'Amare, J. A. Doudna, *Nucleic Acids Res.* **1996**, *24*, 977 – 978.
[21] A. Pingoud, A. Fliess, V. Pingoud, *HPLC of Macromolecules*, IRL Press, Oxford, **1989**.
[22] C. Sich, O. Ohlenschlaeger, R. Ramachandran, M. Goerlach, L. R. Brown, *Biochemistry* **1997**, *36*, 13 989 – 14 002.
[23] M. Stoldt, J. Wöhnert, M. Görlach, L. R. Brown, *EMBO J.* **1998**, *17*, 6377 – 6384.
[24] G. Varani, I. Tinoco, Jr., *Q. Rev. Biophys.* **1991**, *24*, 479 – 532.
[25] K. Wüthrich, *NMR of Proteins and Nucleic Acids*, Wiley, New York, **1986**.
[26] P. R. Schimmel, A. G. Redfield, *Ann. Rev. Biophys. Bioeng.* **1980**, *9*, 181 – 221.
[27] D. R. Kearns, D. J. Patel, R. G. Schulman, *Nature* **1971**, *229*, 338 – 339.
[28] B. R. Reid, N. S. Ribeiro, L. McCollum, J. Abbate, R. E. Hurd, *Biochemistry* **1977**, *16*, 2086 – 2094.
[29] D. R. Kearns, Y. P. Wong, *J. Mol. Biol.* **1974**, *87*, 755 – 774.
[30] M. J. Kime, P. B. Moore, *Biochemistry* **1983**, *22*, 2615 – 2622.
[31] M. J. Kime, P. B. Moore, *Biochemistry* **1983**, *22*, 2622 – 2629.
[32] A. J. Dingley, S. Grzesiek, *J. Am. Chem. Soc.* **1998**, *120*, 8293 – 8297.
[33] K. Pervushin, A. Ono, C. Fernández, T. Szyperski, M. Kainosho, K. Wüthrich, *Proc. Natl. Acad. Sci. USA* **1998**, *95*, 14 147 – 14 151.
[34] G. W. Vuister, A. Bax, *J. Am. Chem. Soc.* **1993**, *115*, 7772 – 7777.
[35] A. Majumdar, A. Kettani, E. Skripkin, D. J. Patel, *J. Biomol. NMR* **1999**, *15*, 207 – 211.
[36] A. Majumdar, A. Kettani, E. Skripkin, *J. Biomol. NMR* **1999**, *14*, 67 – 70.
[37] A. Majumdar, Y. Gosser, D. J. Patel, *J. Biomol. NMR* **2001**, *21*, 289 – 306.
[38] J. Wöhnert, A. J. Dingley, M. Stoldt, M. Görlach, S. Grzesiek, L. R. Brown, *Nucleic Acids Res.* **1999**, *27*, 3104 – 3110.
[39] O. Ohlenschläger, J. Wöhnert, E. Bucci, K. Sidigi, S. Häfner, R. Zell, M. Görlach, unpublished work.
[40] M. Hennig, J. R. Williamson, *Nucleic Acids Res.* **2000**, *28*, 1585 – 1593.
[41] A. J. Dingley, J. E. Masse, R. D. Peterson, M. Barfield, J. Feigon, S. Grzesiek, *J. Am. Chem. Soc.* **1999**, *121*, 6019 – 6027.
[42] A. Liu, A. Majumdar, W. Hu, A. Kettani, E. Skripkin, D. J. Patel, *J. Am. Chem. Soc.* **2000**, *122*, 3206 – 3210.
[43] C. Richter, PhD thesis, University of Frankfurt, Germany, **1999**.
[44] B. Luy, J. P. Marino, *J. Am. Chem. Soc.* **2000**, *122*, 8095 – 8096.
[45] A. J. Dingley, J. E. Masse, J. Feigon, S. Grzesiek, *J. Biomol. NMR* **2000**, *16*, 279 – 289.
[46] D. P. Giedroc, P. V. Cornish, M. Hennig, *J. Am. Chem. Soc.* **2003**, *125*, 4676 – 4677.
[47] C. A. Theimer, L. D. Finger, L. Trantirek, J. Feigon, *Proc. Natl. Acad. Sci. USA* **2003**, *100*, 449 – 454.
[48] C. Richter, PhD. thesis, Johann Wolfgang Goethe University, Frankfurt, Germany, **1999**.
[49] M. Grüne, J. P. Fürste, S. Klussmann, V. A. Erdmann, L. R. Brown, *Nucleic Acids Res.* **1996**, *24*, 2592 – 2596.
[50] E. L. Hahn, *Phys. Rev.* **1950**, *80*, 580 – 594.
[51] E. O. Stejskal, J. E. Tanner, *J. Chem. Phys.* **1965**, *42*, 288 – 292.
[52] J. Lapham, J. P. Rife, P. B. Moore, D. M. Crothers, *J. Biomol. NMR* **1997**, *10*, 255 – 262.
[53] J. H. Cate, R. L. Hanna, J. A. Doudna, *Nat. Struct. Biol.* **1997**, *4*, 553 – 558.
[54] P. Legault, C. G. Hoogstraten, E. Metlitzky, A. Pardi, *J. Mol. Biol.* **1998**, *284*, 325 – 335.
[55] S. E. Butcher, F. H.-T. Allain, J. Feigon, *Biochemistry* **2000**, *39*, 2174 – 2182.
[56] J. S. Kieft, I. J. Tinoco, *Structure* **1997**, *5*, 713 – 721.
[57] M. R. Hansen, J.-P. Simorre, P. Hanson, V. Mokler, L. Bellon, L. Beigelman, A. Pardi, *RNA* **1999**, *5*, 1099 – 1104.
[58] A. Huppler, L. J. Nikstad, A. M. Allmann, D. A. Brow, S. E. Butcher, *Nat. Struct. Biol.* **2002**, *9*, 431 – 435.
[59] F. H.-T. Allain, G. Varani, *Nucleic Acids Res.* **1995**, *23*, 341 – 350.
[60] G. Colmenajero, I. J. Tinoco, *J. Mol. Biol.* **1999**, *290*, 119 – 135.
[61] R. L. J. Gonzalez, I. J. Tinoco, *J. Mol. Biol.* **1999**, *289*, 1267 – 1282.
[62] S. Rüdisser, I. J. Tinoco, *J. Mol. Biol.* **2000**, *295*, 1211 – 1223.
[63] M. Schmitz, I. J. Tinoco, *RNA* **2000**, *6*, 1212 – 1225.
[64] J.-P. Simorre, G. R. Zimmerman, A. Pardi, B. T. I. Farmer, L. Mueller, *J. Biomol. NMR* **1995**, *6*, 427 – 432.
[65] J. S. Simorre, G. R. Zimmerman, L. Müller, A. Pardi, *J. Biomol. NMR* **1996**, *7*, 153 – 156.
[66] V. Sklenar, T. Dieckmann, S. E. Butcher, J. Feigon, *J. Biomol. NMR* **1996**, *7*, 83 – 87.
[67] R. Fiala, F. Jiang, D. J. Patel, *J. Am. Chem. Soc.* **1996**, *118*, 689 – 690.
[68] P. Legault, B. T. Farmer II, L. Mueller, A. Pardi, *J. Am. Chem. Soc.* **1994**, *116*, 2203 – 2204.
[69] J. P. Marino, J. H. Prestegard, D. M. Crothers, *J. Am. Chem. Soc.* **1994**, *116*, 2205 – 2206.
[70] M. v. Dongen, S. Wymengen, R. Eritja, F. Azorin, C. Hilbers, *J. Biomol. NMR* **1996**, *8*, 207.
[71] J. Wöhnert, R. Ramachandran, M. Görlach, L. R. Brown, *J. Magn. Reson.* **1999**, *139*, 430 – 433.
[72] V. Sklenar, J. E. Masse, J. Feigon, *J. Magn. Res.* **1999**, *137*, 345 – 349.
[73] J. Wöhnert, M. Görlach, H. Schwalbe, *J. Biomol. NMR* **2003**, *26*, 79 – 83.
[74] G. Varani, I. J. Tinoco, *J. Am. Chem. Soc.* **1991**, *113*, 9349 – 9354.
[75] L. Mueller, P. Legault, A. Pardi, *J. Am. Chem. Soc.* **1995**, *117*, 11 043 – 11 048.
[76] C. Zwahlen, P. Legault, S. Vincent, J. Greenblatt, R. Kourat, L. E. Kay, *J. Am. Chem. Soc.* **1997**, *119*, 6711 – 6721.
[77] V. Sklenar, R. D. Peterson, M. R. Rejante, J. Feigon, *J. Biomol. NMR* **1993**, *3*, 721 – 727.
[78] B. T. Farmer II, L. Mueller, E. P. Nikonowicz, A. Pardi, *J. Biomol. NMR* **1994**, *4*, 129 – 133.
[79] J. P. Marino, J. L. Diener, P. B. Moore, C. Griesinger, *J. Am. Chem. Soc.* **1997**, *119*, 7361 – 7366.
[80] V. Sklenar, T. Dieckmann, S. E. Butcher, J. Feigon, *J. Magn. Reson.* **1998**, *130*, 119 – 124.
[81] R. Fiala, J. Czernek, V. Sklenar, *J. Biomol. NMR* **2000**, *16*, 291 – 302.
[82] B. Brutcher, J.-P. J. Simorre, *J. Biomol. NMR* **2001**, *21*, 367 – 372.
[83] S. Grzesiek, A. Bax, *J. Biomol. NMR* **1995**, *4*, 325 – 332.
[84] V. Sklenar, M. R. Rejante, R. D. Peterson, E. Wang, J. Feigon, *J. Am. Chem. Soc.* **1993**, *115*, 12 181 – 12 182.
[85] B. T. Farmer II, L. Muller, E. P. Nikonowicz, A. Pardi, *J. Am. Chem. Soc.* **1993**, *115*, 11 040 – 11 041.
[86] V. Sklenar, R. D. Peterson, M. R. Rejante, J. Feigon, *J. Biomol. NMR* **1994**, *4*, 117 – 122.
[87] D. R. Muhandiram, L. E. Kay, *J. Magn. Reson. Ser. B* **1994**, *103*, 203 – 216.
[88] H. Schwalbe, J. P. Marino, S. J. Glaser, C. Griesinger, *J. Am. Chem. Soc.* **1995**, *117*, 7251 – 7252.
[89] J. P. Marino, H. Schwalbe, S. J. Glaser, C. Griesinger, *J. Am. Chem. Soc.* **1996**, *118*, 4388 – 4395.
[90] S. J. Glaser, H. Schwalbe, J. P. Marino, C. Griesinger, *J. Magn. Reson.* **1996**, *B112*, 160 – 180.
[91] A. Pardi, E. P. Nikonowicz, *J. Am. Chem. Soc.* **1992**, *114*, 9202 – 9203.
[92] H. A. Heus, S. S. Wijmenga, F. J. M. van de Ven, C. W. Hilbers, *J. Am. Chem. Soc.* **1994**, *116*, 4983 – 4984.
[93] R. Ramachandran, C. Sich, M. Grüne, V. Soskic, L. R. Brown, *J. Biomol. NMR* **1996**, *7*, 251 – 255.
[94] J. P. Marino, H. Schwalbe, C. Anklin, W. Bermel, D. M. Crothers, C. Griesinger, *J. Am. Chem. Soc.* **1994**, *116*, 6472 – 6473.
[95] J. P. Marino, H. Schwalbe, C. Anklin, W. Bermel, D. M. Crothers, C. Griesinger, *J. Biomol. NMR* **1995**, *5*, 87 – 92.

 © 2003 Wiley-VCH Verlag GmbH & Co. KGaA, Weinheim

[96] J. A. M. T. C. Cromsigt, C. W. Hilbers, S. S. Wijmenga, *J. Biomol. NMR* **2001**, *21*, 11 – 29.
[97] M. Ebrahimi, P. Rossi, C. Rogers, G. S. Harbison, *J. Magn. Reson.* **2001**, *150*, 1 – 9.
[98] M. Remin, D. Shugar, *Biochem. Biophys. Res. Commun.* **1972**, *48*, 636 – 642.
[99] F. M. Jucker, H. A. Heus, P. F. Yip, E. H. M. Moors, A. Pardi, *J. Mol. Biol.* **1996**, *264*, 968 – 980.
[100] A. A. Szewczak, P. B. Moore, *J. Mol. Biol.* **1995**, *247*, 81 – 98.
[101] A. A. Szewczak, P. B. Moore, Y.-L. Chan, I. G. Wool, *Proc. Natl. Acad. Sci. USA* **1993**, *90*, 9581 – 9585.
[102] B. Wimberly, *Nat. Struct. Biol.* **1994**, *1*, 820 – 827.
[103] B. Wimberly, G. Varani, I. J. Tinoco, *Biochemistry* **1993**, *32*, 1078 – 1087.
[104] A. Dallas, P. B. Moore, *Structure* **1997**, *5*, 1639 – 1653.
[105] S. E. Butcher, J. M. Burke, *Biochemistry* **1994**, *33*, 992 – 999.
[106] A. D. Branch, B. J. Benenfeld, H. D. Robertson, *Proc. Natl. Acad. Sci. USA* **1985**, *82*, 6590 – 6594.
[107] C. A. G. Haasnoot, F. A. A. M. De Leeuw, C. Altona, *Tetrahedron* **1980**, *36*, 2783 – 2792.
[108] C. A. G. Haasnoot, F. A. A. M. de Leeuw, H. P. M. de Leeuw, C. Altona, *Org. Magn. Reson.* **1981**, *15*, 43 – 52.
[109] C. A. G. Haasnoot, F. A. A. M. de Leeuw, H. P. M. de Leeuw, C. Altona, *Biopolymers* **1981**, *20*, 1211 – 1216.
[110] E. Duchardt, C. Richter, B. Reif, S. J. Glaser, J. W. Engels, C. Griesinger, H. Schwalbe, *J. Biomol. NMR* **2001**, *21*, 117 – 126.
[111] I. C. Felli, C. Richter, C. Griesinger, H. Schwalbe, *J. Am. Chem. Soc.* **1999**, *121*, 1956 – 1957.
[112] H. Schwalbe, T. Carlamango, M. Hennig, J. Junker, B. Reif, C. Richter, C. Griesinger, *Meth. Enzymol.* **2001**, *338*, 35 – 81.
[113] C. Griesinger, M. Hennig, J. P. Marino, B. Reif, C. Richter, H. Schwalbe, *Modern Techniques in Protein NMR* **1999**, *16*, 259 – 367.
[114] M. R. Hansen, L. Mueller, A. Pardi, *Nat. Struct. Biol.* **1998**, *5*, 1065 – 1074.
[115] M. Rückert, G. Otting, *J. Am. Chem. Soc.* **2000**, *122*, 7793 – 7797.
[116] T. C. Leeper, M. B. Martin, H. Kim, S. Cox, V. Semenchenko, F. J. Schmidt, S. R. Van Doren, *Nat. Struct. Biol.* **2002**, *9*, 397 – 403.
[117] R. D. Beger, V. M. Marathias, B. F. Volkman, P. H. Bolton, *J. Magn. Reson.* **1998**, *135*, 256 – 259.
[118] B. N. M. van Buuren, J. Schleucher, V. Wittmann, C. Griesinger, H. Schwalbe, S. S. Wijmenga, unpublished work.
[119] J. J. Warren, P. B. Moore, *J. Biomol. NMR* **2001**, *20*, 311 – 323.
[120] S. A. McCallum, A. Pardi, *J. Mol. Biol.* **2003**, *326*, 1037 – 1050.
[121] P. Vallurupalli, P. B. Moore, *J. Mol. Biol.* **2003**, *325*, 843 – 856.
[122] D. C. Lawrence, C. C. Stover, J. Noznitsky, Z. Wu, M. F. Summers, *J. Mol. Biol.* **2003**, *326*, 529 – 542.
[123] M. Hennig, T. Carlamango, J. R. Williamson, *J. Am. Chem. Soc.* **2001**, *123*, 3395 – 3396.
[124] M. R. Hansen, M. Rance, A. Pardi, *J. Am. Chem. Soc.* **1998**, *120*, 11 210 – 11 211.
[125] P. Bayer, L. Varani, G. Varani, *J. Biomol. NMR* **1999**, *14*, 149 – 155.
[126] N. Sibille, A. Pardi, J.-P. Simorre, M. Blackledge, *J. Am. Chem. Soc.* **2001**, *123*, 12 135 – 12 146.
[127] E. T. Mollova, M. R. Hansen, A. Pardi, *J. Am. Chem. Soc.* **2000**, *122*, 11 561 – 11 562.
[128] K. Bodensgaard, E. T. Mollova, A. Pardi, *Biochemistry* **2002**, *41*, 11 532 – 11 542.
[129] H. M. Al-Hashimi, A. Gorin, A. Majumdar, D. J. Patel, *J. Am. Chem. Soc.* **2001**, *123*, 3179 – 3180.
[130] H. M. Al-Hashimi, Y. Gosser, A. Gorin, W. Hu, A. Majumdar, D. J. Patel, *J. Mol. Biol.* **2002**, *315*, 95 – 102.
[131] H. M. Al-Hashimi, A. Gorin, A. Majumdar, Y. Gosser, D. J. Patel, *J. Mol. Biol.* **2002**, *318*, 631 – 649.
[132] M. Stoldt, J. Wöhnert, O. Ohlenschläger, M. Görlach, L. R. Brown, *EMBO J.* **1999**, *18*, 6508 – 6521.
[133] M. Lu, T. A. Steitz, *Proc. Natl. Acad. Sci. USA* **2000**, *97*, 2023 – 2028.
[134] Y. Yang, N. Declerck, X. Manival, S. Aymerich, M. Kochoyan, *EMBO J.* **2002**, *21*, 1987 – 1997.
[135] P. W. Howe, K. Nagai, D. Neuhaus, G. Varani, *EMBO J.* **1994**, *13*, 3873 – 3881.
[136] D. Fourmy, E. Guittet, S. Yoshizawa, *J. Mol. Biol.* **2002**, *324*, 137 – 150.
[137] I. Lebars, S. Yoshizawa, A. R. Stenholm, E. Guittet, S. Douthwaite, D. Fourmy, *EMBO J.* **2003**, *22*, 183 – 192.
[138] H. Takahashi, T. Nakanishi, K. Kami, Y. Arata, I. Shimada, *Nat. Struct. Biol.* **2000**, *7*, 220 – 223.
[139] A. Ramos, G. Kelly, D. Hollingworth, A. Pastore, T. A. Frenkiel, *J. Am. Chem. Soc.* **2000**, *122*, 11 311 – 11 314.
[140] A. Lane, G. Kelly, A. Ramos, T. A. Frenkiel, *J. Biomol. NMR* **2001**, *21*, 127 – 139.
[141] C. Richter, B. Reif, C. Griesinger, H. Schwalbe, *J. Am. Chem. Soc.* **2000**, *122*, 12 728 – 12 731.
[142] H. Schwalbe, W. Samstag, J. W. Engels, W. Bermel, C. Griesinger, *J. Biomol. NMR* **1993**, *3*, 479 – 486.
[143] H. Schwalbe, J. P. Marino, G. C. King, R. Wechselberger, W. Bermel, C. Griesinger, *J. Biomol. NMR* **1994**, *4*, 631 – 644.
[144] P. Legault, F. M. Jucker, A. Pardi, *FEBS Lett.* **1995**, *362*, 156 – 160.
[145] C. Richter, B. Reif, K. Worner, S. Quant, J. P. Marino, J. W. Engels, C. Griesinger, H. Schwalbe, *J. Biomol. NMR* **1998**, *12*, 223 – 230.
[146] W. Hu, S. Bouaziz, E. Skripkin, A. Kettani, *J. Magn. Res.* **1999**, *139*, 181 – 185.
[147] T. Carlamango, M. Hennig, J. R. Williamson, *J. Biomol. NMR* **2002**, *22*, 65 – 81.
[148] J. V. Hines, G. Varani, S. M. Landry, I. Tinoco, Jr., *J. Am. Chem. Soc.* **1993**, *115*, 11 002 – 11 003.
[149] V. Sklenar, A. Bax, *J. Am. Chem. Soc.* **1987**, *109*, 7525 – 7526.
[150] G. M. Clore, E. C. Murphy, A. M. Gronenborn, A. Bax, *J. Magn. Res.* **1998**, *134*, 164 – 167.
[151] L. Trantirek, R. Stefl, J. E. Masse, J. Feigon, V. Sklenar, *J. Biomol. NMR* **2002**, *23*, 1 – 20.
[152] E. Duchardt, C. Richter, O. Ohlenschlaeger, M. Görlach, J. Wöhnert, H. Schwalbe, *J. Am. Chem. Soc.* **2003**, in press.
[153] C. Richter, C. Griesinger, I. C. Felli, P. T. Cole, G. Varani, H. Schwalbe, *J. Am. Chem. Soc.* **1999**, *121*, 1956 – 1957.
[154] R. Riek, *J. Magn. Res.* **2001**, *149*, 149 – 153.
[155] E. Chiarparin, S. Rüdisser, G. Bodenhausen, *ChemPhysChem* **2001**, *2*, 41 – 45.

Received: June 24, 2003 [A 700]

 © 2003 Wiley-VCH Verlag GmbH & Co. KGaA, Weinheim